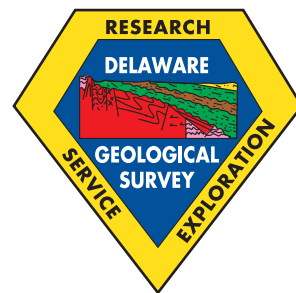


State of Delaware
DELAWARE GEOLOGICAL SURVEY
David R. Wunsch, State Geologist

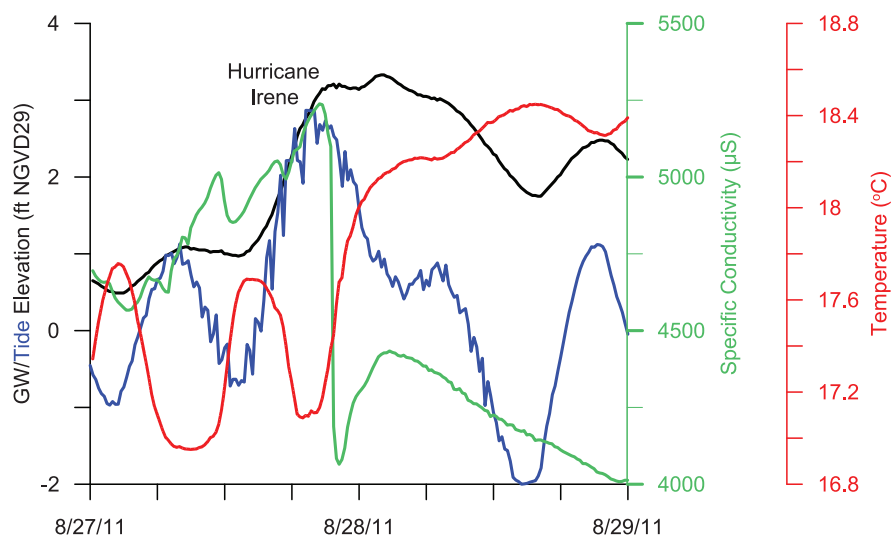


REPORT OF INVESTIGATIONS NO. 80

INVESTIGATION OF SUBMARINE GROUNDWATER DISCHARGE AT HOLTS LANDING STATE PARK, DELAWARE: HYDROGEOLOGIC FRAMEWORK, GROUNDWATER LEVEL AND SALINITY OBSERVATIONS

By:

A. Scott Andres¹, Holly Michael²,
Christopher J. Russoniello²,
Cristina Fernandez², Changming He¹, and John A. Madsen²



University of Delaware
Newark, Delaware
2017

¹ Delaware Geological Survey

² University of Delaware, Department of Geological Sciences

TABLE OF CONTENTS

	Page
ABSTRACT	1
INTRODUCTION	1
Purpose and Scope	1
Previous Work	1
Acknowledgments	2
METHODS	2
Locaton and Vertical Positions/Data Management	2
Subsurface Exploration	3
Well Design and Installation	4
Hydraulic Tests	5
Weather/Water Level/Temperature/Specific Conductance Monitoring	5
RESULTS AND DISCUSSION	5
Litho- and Hydrostratigraphy	5
Hydrologic and Hydraulic Observations	11
Tidal Effects	14
Freshwater – Saltwater Interface	15
CONCLUSIONS	18
REFERENCES CITED	19
APPENDICES	21

ILLUSTRATIONS

	Page
Figure 1. Location of the study area.....	2
Figure 2. Site map.....	3
Figure 3. Well installation, offshore drilling, and offshore wellhead components	4-5
Figure 4. Geophysical and descriptive logs for test borings	7-8
Figure 5. Interpreted 1937 aerial photograph.....	9
Figure 6. Interpretive cross sections.....	9-10
Figure 7. A core through Holocene marsh deposits, and modern marsh landscape	11
Figure 8. Groundwater levels and temperatures from selected inland wells, and precipitation at Georgetown, DE.....	11
Figure 9. Groundwater levels, temperatures, and specific conductivity from selected near shore and bay wells.....	12
Figure 10. Comparison of groundwater temperatures and specific conductivities between inland, shoreline, and offshore wells	13
Figure 11. Examples of response of head, temperature, and specific conductivity to tides	15
Figure 12. Interpretive cross-sectional view of fresh water-salt water interface at Holts Landing State Park.....	16
Figure 13. Comparison of hydrologic forcing and specific conductivity response	17
Figure 14. Head, temperature, and specific conductivity variations during Hurricane Irene at wells Pi53-52 and Qi13-06, and tide elevations.....	18
Figure 15. Head, tide height, and specific conductivity variations during a high tide event in June 2012	18

TABLES

	Page
Table 1. Hydraulic conductivity (K) determined by slug-test methods in project wells	12
Table 2. Vertical gradient data.....	12
Table 3. Timing of temperature maxima and minima.....	14
Table 4. Tidal efficiency of wells	15
Table 5. Comparison of conductivity and specific conductivity (SC) at well cluster 3	15

APPENDICES

Appendix A. Attributes of wells installed at Holts Landing State Park.....	21
Appendix B. Hydrographs, thermographs, and specific conductivity time series	23

INVESTIGATION OF SUBMARINE GROUNDWATER DISCHARGE AT HOLTS LANDING STATE PARK, DELAWARE: HYDROGEOLOGIC FRAMEWORK, GROUNDWATER LEVEL AND SALINITY OBSERVATIONS

ABSTRACT

Monitoring wells and groundwater sensors were installed and monitored in and around Holts Landing State Park on the Indian River Bay, eastern Sussex County, Delaware, between October 2009 and August 2012. Data from test drilling, geophysical logging, geophysical surveys, and well testing characterized the hydrogeological framework and spatial and temporal patterns of water pressure, temperature, and salinity in the shallow, unconfined Columbia aquifer. The work revealed a plume of freshened groundwater extending more than 650 ft into the bay from the shoreline. Groundwater salinities intermediate between baywater and inland groundwater are present both offshore and on land adjacent to the bay and tidal tributaries.

The fresh groundwater plume, as observed in wells and borehole geophysical logs, decreases in thickness from more than 40 ft nearest the shoreline to less than 20 ft farthest from the shoreline. Saline water is found above and below the plume and the freshwater-saltwater interface is spatially complex. Characterization of the hydrogeologic framework was critical to explaining the distribution of fresh groundwater. Fresh water is trapped near the bay bottom by an overlying confining bed composed of the low permeability sediments of a Holocene paleovalley fill sequence and the Beaverdam Formation. This complex, heterogeneous geological framework also causes multiple stacked interfaces in one location at the study site.

Groundwater levels, temperatures, and specific conductivity respond to climatic, seasonal, and storm-related weather forcing patterns as well as to forces caused by astronomical tides. The relative importance of these forces to groundwater levels, the flux of fresh groundwater, and groundwater salinity varies with location. Ranges in groundwater levels are more than 6 ft at an inland location and are clearly controlled by seasonal recharge patterns. Extreme weather events have a secondary effect on groundwater levels. In comparison, ranges of groundwater levels are much smaller in near shore and offshore wells, and are more closely related to tidal forces. As a result of this difference in ranges of groundwater levels, seasonal variations in water levels at inland locations are the primary variable controlling bayward-directed groundwater gradients, fresh groundwater flux, and groundwater salinity distribution. Shorter duration weather and tidal events have a secondary role. The freshwater-saltwater interface and associated mixing zone moves upward and/or landward during extended periods of low freshwater flux into the bay, and downward and/or bayward during extended periods of higher freshwater flux.

INTRODUCTION

Groundwater discharge into estuaries and coastal oceans carries fresh water, but also nitrogen (N) and phosphorus (P), which can lead to serious eutrophication (Johannes, 1980; Vitousek and Aber, 1997; DNREC, 1998; Slomp and van Cappellen, 2004; Selman and Greenhalgh, 2007). To develop strategies and management tools to mitigate this problem, it is necessary to characterize the processes controlling transport of N and P by groundwater. Such characterization of groundwater flow requires investigation of subsurface geologic materials and waters, which is commonly done through test boring, geophysics, installation of sampling devices, and sampling physical and chemical properties of groundwater.

Purpose and Scope

This report describes the methods and results of a hydrogeologic study conducted in 2009-2012 by the Delaware Geological Survey (DGS) and University of Delaware Department of Geological Sciences (UDDoGS). The study area is the land and waters at Holts Landing State Park (HLSP), located in the Inland Bays region of Sussex County, Delaware (Figs. 1 and 2). This National Science Foundation-funded work was part of a larger project led by Dr. Holly Michael of UDDoGS and included faculty and student collaborators from UDDoGS and the Department of Earth

Sciences at the University of Toledo (UTES), and the research staff of the US Geological Survey (USGS). The work analyzes the surface and subsurface materials derived from test drilling, coring, and downhole geophysical logging, plus observations of outcrops collected by UDDoGS and DGS during the current project, and by DGS and others in previous studies. Interpretations of project observations were supplemented by an analysis of the seismic data collected by UTES and USGS. N and P results are discussed in Fernandez (2012).

Previous Work

Much of this study relies on prior interpretations of the geological history and hydrogeological framework of the Inland Bays region. Chrzastowski (1986) found that the Indian River Bay is underlain by Holocene tidal channel, flat, beach, and marsh sediments deposited in a paleo-drainage system that was cut during the Wisconsinan glaciation. The sediments form a paleovalley fill (PVF) sequence. The region is a drowned estuary in which the sub-environments migrated upward and landward as sea level rose nearly 200 ft since the Wisconsin glacial maximum. Subsequent work by Williams (1999), McKenna and Ramsey (2002), Krantz et al. (2004), and Brown (2006) refined the locations and geometries of the main and tributary paleovalleys and the composition of the PVF sediments.

The late Pleistocene and Holocene deposits that unconformably overlie older marginal marine and marine deposits are within the Pleistocene Sinepuxent, Ironshire, and Omar Formations, and Plio-Pleistocene (?) Beaverdam Formation (Tomlinson et al., 2013; Andres and Klingbeil, 2006). The water-bearing zones included in these units are assigned to the Columbia aquifer (Andres and Klingbeil, 2006). Detailed descriptions of the composition and depositional environments and hydraulic properties associated with these lithostratigraphic units will be discussed in the results section.

Earlier research on submarine groundwater discharge (SGD) in the Delaware Inland Bays region (Stegner, 1972; Lauffer, 1982; and Andres, 1987) noted the presence of fresh groundwater near the shorelines and under the bays, and postulated that high rates of fresh groundwater flux toward the bays and the presence of fine-grained bay-bottom sediments may promote fresh SGD. Subsequent test borings and seismic reflection and continuous resistivity profile (CRP) surveys conducted by Bratton et al. (2004), Krantz et al. (2004), and Manheim et al. (2004) found relatively fresh groundwater beneath Indian River Bay in locations hundreds of feet offshore and tens of feet beneath the bay bottom. The researchers postulated that the fine-grained PVF sediments function as a confining bed or cap that restricts fresh water from discharging into the bay at the shoreline. This causes a plume of fresh water to travel offshore and discharge around the cap. The researchers also identified that salt water underlying the freshwater plume is younger than the water in the freshwater plume. Although they suggested that the freshwater plume is driving a hydrodynamically-complex rapid saline circulation cell, they did not have adequate data to verify this hypothesis. A related effort (Russoniello et al., 2013) conducted in coordination with this study refined the understanding of the spatial distribution and geometry of near bottom fine-grained sediments and confirmed that the rate and salinity of SGD at HLSP is clearly related to the distribution and geometry of these sediments. In a companion study, Fernandez (2012) investigated groundwater quality at Holts Landing using the wells installed for the current study and found fresh groundwater in multiple offshore wells. The goal of this study is to further investigate the effects of geologic heterogeneity on the flux of fresh groundwater to the bay by characterizing the deeper flow system and geochemistry associated with these fresh and saline groundwaters at Holts Landing State Park (Fig. 2).

Acknowledgments

Primary funding for this project was from the National Science Foundation (NSF) for “Quantifying Geologic and Temporal Controls on Water and Chemical Exchange between Groundwater and Surface Water in Coastal Estuarine Systems” (NSF 0910756/6848526). We thank Andrew Musetto, Kevin Myers, of UD, Leonard Konikow of the USGS, and Christopher Bason of the Center for the Inland Bays (CIB) for their participation in drilling crews and assistance with logistics. Edward Walther, Jaime Tomlinson, Kelvin Ramsey, and Thomas McKenna of the DGS are thanked for their participation in the drilling

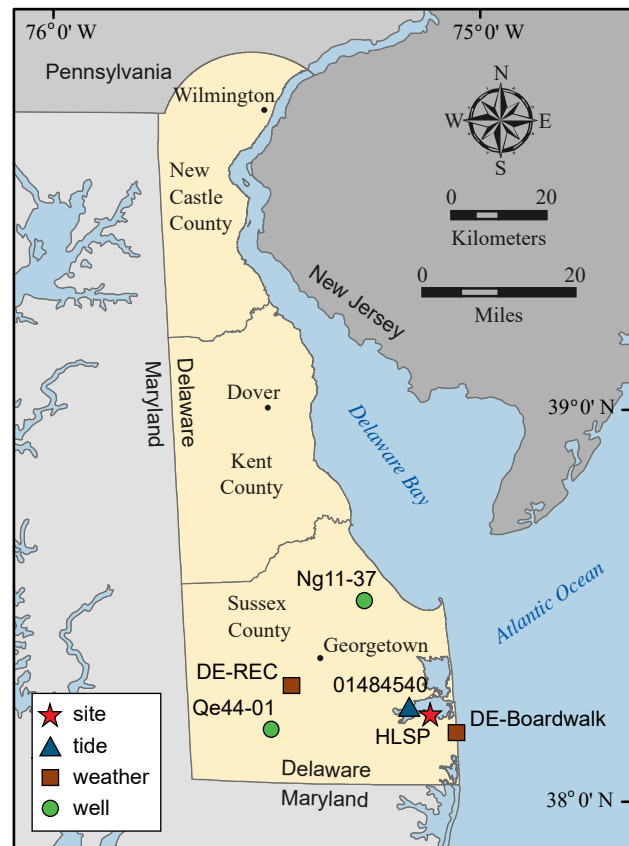


Figure 1. Location of the study area. Town, state, and water body names are provided for spatial reference. Symbols denote features described in the text. HLSP- Holts Landing State Park.

operations. P. Stephen McCreary was the licensed water well driller and chief mechanic responsible for all drilling operations. Steven Smaller provided photographs of offshore drilling operations. The Walton Corporation of Newark, Delaware loaned a pontoon boat, tripod, gasoline-powered hoist, and coring hammer for use in the drilling program and provided advice on logistics and drilling methods.

Multiple programs with the Delaware Department of Natural Resources and Environmental Control (DNREC) including Water Supply Section, Subaqueous Lands Section, and Division of Parks and Recreation issued the necessary permits. We are especially grateful to the Division of Parks and Recreation for providing essential logistical support at HLSP. Additional financial support was provided by the DGS and the Undergraduate Internship program of the UD Water Resources Center.

METHODS

Locational and Vertical Positions/Data Management

Horizontal positions of individual wells, test borings, and outcrops were derived by hand-held GPS with WAAS correction. Vertical control for well casing measurement points were determined by a double-loop auto-level survey using a State of Delaware-installed benchmark located in the study area and tied to NGVD 1929. On closure, errors were less than 0.01 ft. Vertical positions of other features on land were determined by GIS analysis of a LiDAR-DEM (USGS, 2005) and converted to NGVD 1929 with Corpcon (USACE, 2004).

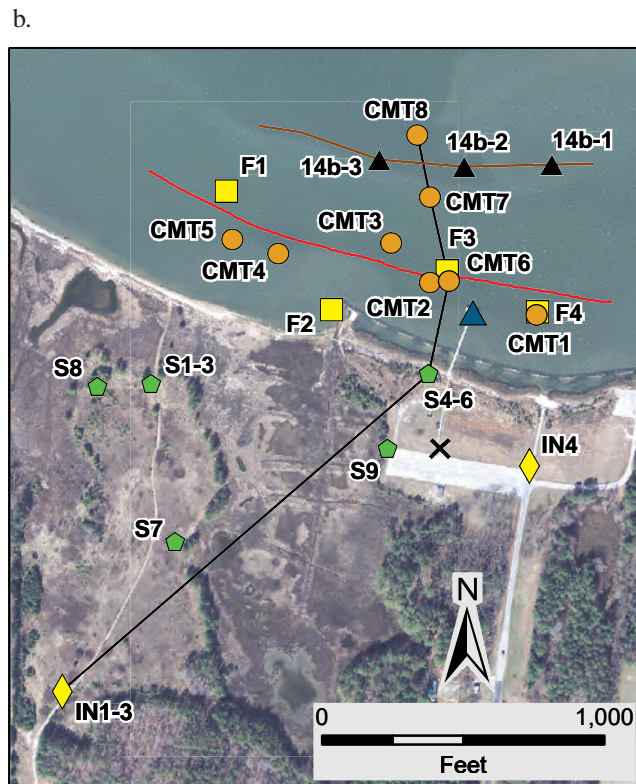
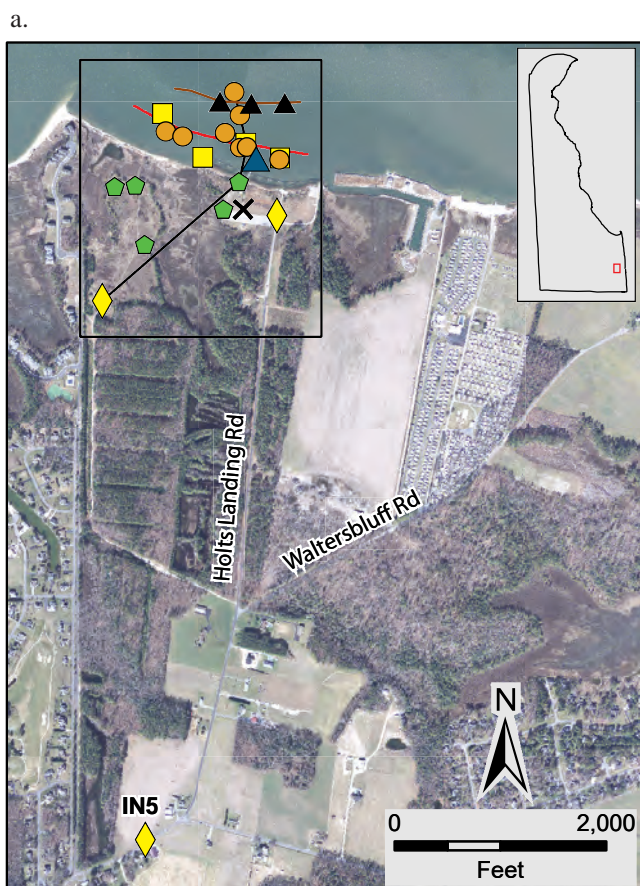


Figure 2. Site map.

(a) Holts Landing State Park and vicinity showing selected wells, line of cross section, and seismic line described in report.

(b) A close-up of the study site showing well and site identifiers. Locations were chosen to determine groundwater flow directions and to characterize interactions between the bay and aquifer. Appendix A contains a listing of well construction and labeling data.

ArcGIS (ESRI, 2012) was used for data visualization, quality assurance/quality control (QA/QC) of horizontal coordinates, and the development of cartographic products and topographic profiles from the DEM. Grapher (Golden Software, 2011) was used to develop cross sections. Data presented in this report have been entered into the DGS institutional database management system.

Subsurface Exploration

Onshore boreholes and wells were constructed using the DGS truck-mounted hollow stem auger (HSA) drilling system. Cores were collected at several test-boring sites using a 2.25-inch inside diameter (ID) HSA with continuous standard split barrel coring of the uppermost 15 to 30 ft, then coring at 5-ft intervals to total depth. Offshore borings were constructed standard hydraulic rotary drilling (Sterrett, 2008) methods. The drilling system (Fig. 3a) was constructed by project personnel and consisted of the following components:

22-ft Pontoon Boat: modified with four spuds for anchoring

Electric: 2000-watt gasoline powered generator

Hoist: gasoline powered cathead

Rotary: electric powered pipe threader

Drill Rod: various lengths of 1.5-inch ID galvanized pipe, couplings, and various threaded adaptors to connect the drill bit to the rods and the rods to the rotary power

Mud Circulation: 8-horsepower gasoline powered centrifugal pump

Drill Bit: tri-cone roller

Riser: 6-inch and 8-inch schedule 40 PVC pipes, couplings, and T fittings

Various hand tools

Standard split barrel system: sampling rods, tubes, and 150-lb hammer

Support boats: 12-ft johnboat and 16-ft Carolina skiff

Drilling fluid was formulated from fresh water and sodium bentonite, with soda ash and polymer additives to keep proper mud viscosity. A riser-pipe extending from about 5 to 8 ft below the bay bottom to the on-deck mud pit was used to stabilize the tops of the holes, carry cuttings to

a.



Figure 3a. Well installation, offshore drilling, and offshore well-head components on the offshore drilling barge.

the mud pit, and allow recirculation of drilling fluids. Samples of soft, sub-bottom sediments were collected using standard split-barrel coring techniques.

Downhole geophysical logs were collected with a DGS-owned Century System 6. In HSA test borings, a natural gamma radiation tool (Century 9012A) was used. An EM conductivity-natural gamma tool (Century 9512A) was used in open holes drilled by mud rotary and in PVC-cased wells. Descriptive lithologic logs were constructed from interpretations of cores, cuttings, and geophysical logs. Sediment colors were keyed to a standard color chart (Rock Color Chart Committee, 1979). Geophysical and descriptive logs are archived in the DGS institutional database management system and are available for viewing in the web-based Delaware Geologic Information Resource (DGIR) application at maps.dgs.udel.edu.

Well Design and Installation

Well borings were constructed with a 4.25-inch ID HSA, then constructed through the HSA with 2-inch schedule 40 PVC, flush-threaded casing. Each well had 5 ft of screen. First a gravel pack and then 2 to 3 ft of pelleted bentonite were gravity-placed through the HSA to 2 ft above the screen. Additional grout was emplaced through the HSA as the HSA was pulled from the ground. For all well constructions, depth soundings located the top of gravel and/or bentonite to ensure proper emplacement of the gravel pack and grout. Protective metal covers were placed over the well-heads. Lastly, the wells were over-pumped for 1 to 2 hours to clear the screens of fine-grained sediment.

Following completion of borings at four offshore locations, standard 2-inch ID wells (5-ft screen length) were assembled on barge and inserted in the open hole. Gravel pack was gravity placed to 5 ft above screen interval, and chipped bentonite grout was then gravity placed from the top of the gravel pack to the bay bottom. During this process, the hole depth was sounded, as described above. Wellheads, consisting of a water-tight telescoping assembly (Fig. 3b), were inserted into the hole until flush with the bay bottom. The telescoping portion of the well head can be pulled above the water surface to measure total head and to insert data-logging instruments.

Continuous multichannel tube (CMT) wells (Einarson and Cherry, 2004), which allow multiple sampling ports in an individual borehole, were installed at eight offshore locations. Sampling port depths were pre-determined from

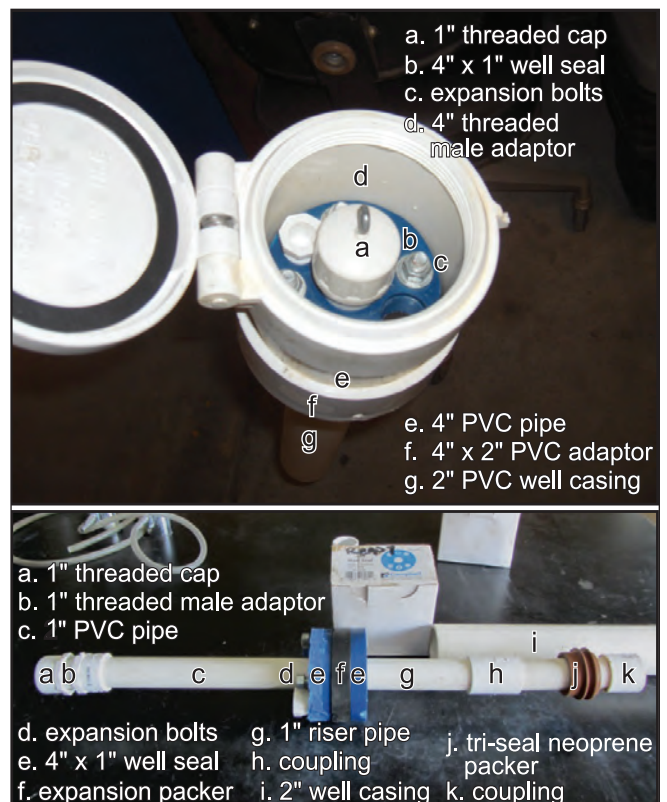


Figure 3b. Top and lateral views of telescoping well-head system view of wellhead assembly used in offshore wells. The system and well were inserted into a completed borehole and mounted flush with the bay bottom.



Figure 3c. Installation of CMT well from offshore drilling barge.

the evaluation of CRP and seismic data. Following the completion of a mud-rotary boring, a pre-assembled 7-channel CMT well (Fig. 3c) was transported to the drilling barge and inserted into the open hole. Sampling port depths were guided by the results of the CRP survey and data from wells and CMT installations earlier in the project. Gravel pack was emplaced from the top of the riser pipe to 2 to 5 ft above the shallowest sample port; chipped bentonite then was placed to the bay bottom. Each channel of the CMT was constructed with a water-tight wellhead (rubber gasket and epoxy) and sampling tubes that can be extended above bay level. Each tube was sealed with an oversized threaded bolt that can be removed for sampling. Each CMT was fit with a protective surface cover.

A total of seven test borings and 17 standard single-screen wells were completed on land and offshore at HLSP (Fig. 2, Appendix A). Local identifiers that include indication of the well type and position along with a serial component (e.g., 1, 2, 3, etc.) were created for discussion and illustrative purposes in this report. Wells located on land within 25 ft of the edge of the marsh or bay will be identified as shoreline (S). Wells located on land more than 25 ft from the edge of the marsh or bay will be identified as inland (IN). Standard wells located in the bay will be identified as offshore (F). CMT wells are identified CMT. These identifiers are listed in Appendix A and locations shown on Figure 2. Clusters of three standard wells were installed at three sites. Seven-channel, CMT, multi-depth sampling systems (Einarson and Cherry, 2002) were installed at eight offshore locations (Fig. 2). Geophysical logs were run at the three on-land, well-cluster sites (IN1-3, S1-3, S4-6) and three of the offshore CMT locations (CMT6-8).

Hydraulic Tests

Single well aquifer tests (slug tests) were conducted in onshore monitoring wells following guidelines in Butler (1996) to determine hydraulic conductivity (K). Water was displaced with a mechanical slug constructed from a sealed, 0.75-inch ID sand-filled, PVC pipe, and nylon cord. Change in head was measured and recorded with an In-Situ Level

Troll 700 relative pressure transducer/data logger. The recording interval ranged from 0.25 sec to 1 sec depending on the well. Three replicate tests were conducted in each well and the rising head portions of the tests were analyzed using Aquifer Test Pro (SWS, Inc. 2011) software. Data from nearly all wells showed a normally damped response and were analyzed by the Bouwer and Rice (Bouwer, 1989) method. One well showed an under-damped response and was analyzed by the high-K method introduced in Butler (1996).

Weather/Water Level/Temperature/Specific Conductance Monitoring

Weather (e.g., precipitation and temperature) data were acquired from station DE-REC operated by the Delaware Environmental Observing System (DEOS, <http://www.deos.udel.edu/>; Fig. 1). Ambient groundwater and baywater levels, temperature, and specific conductance were monitored in project wells and a surface-water monitoring station using manual and automated methods. Manual water level readings were made with electronic water-level meters with 0.01-ft gradations. Automated measurements were collected at 15-min intervals with absolute-type In-Situ Level Troll models 300 and 500 (approximately 33-ft range) and In-Situ AquaTroll 200 (approximately 190-ft range) instruments. Pressure and temperature systems were calibrated by the manufacturer. The specific conductance sensor of the AquaTroll was calibrated with solutions sold by the manufacturer prior to deployments. Heads were corrected for salinity when appropriate. Barometric corrections to heads were derived from data collected from the DEOS weather station DE-Boardwalk (<http://www.deos.udel.edu/>). Temperature data from sensors deployed within the well screen intervals were saved for further evaluation. Data were visually screened for outliers and instrument malfunction and those points were removed from further analyses. The elevation of the bay monitoring instrument was not surveyed; all tidal elevations are approximated by correlation with tidal records collected at USGS station 01484540 (<http://waterdata.usgs.gov/usa/nwis/uv?01484540>), located just northwest of HLSP (Fig. 1). The bay monitoring instrument was above water level during extreme low tides on multiple dates and these data were excluded from further analysis.

RESULTS AND DISCUSSION

Interpretations of lithostratigraphy were done in parallel with a previous subsurface mapping project (Andres and Klingbeil, 2006) and previous geologic mapping projects (Ramsey, 2011; Ramsey and Tomlinson, 2011, 2012), as well as a parallel geologic mapping project (Tomlinson et al., 2013). Lithostratigraphic interpretations were informed by seismic reflection data collected by Banaszak (2011) and Cross et al. (2013).

Litho- and Hydrostratigraphy

Analysis of lithologic and geophysical logs (Figs. 4a-4f) reveals the presence of several lithostratigraphic units, hydraulic fill, modern bay-bottom deposits, Holocene marsh and bay-bottom deposits, the Beaverdam Formation, and the Bethany Formation. About 12 ft of thinly bedded sand and

organic silt in borings at sites Pi53-13 (S9) and Pi53-10 (S4) that were identified as hydraulic fill are currently on fast land, but were in the tidal marsh in a 1937 aerial photograph (Fig. 5). The Beaverdam Formation was the thickest and most frequently penetrated unit during test drilling, extending from near land surface or bay bottom to a depth of approximately 95 ft at Pi53-10 (S4, Fig. 4c). Where present the Holocene units range from about 1 ft to about 10 ft, with the thickest accumulations appearing under the present-day marsh and the extension of the paleo-marsh under the modern bay (Banaszak, 2011; Russoniello et al., 2013).

Sandier deposits of the Beaverdam Formation and Holocene bay-bottom deposits form the Columbia aquifer at the site (Figs. 4, 6a). Although the Beaverdam Formation is predominately sandy, its lithology is highly heterogeneous both horizontally and vertically, with lithologies ranging from beds of sandy mud to sand and gravel. The muddier deposits of the modern bay bottom, Holocene marsh and lagoon, and the uppermost Beaverdam Formation form an overlying leaky confining unit. Muddy beds of the underlying Bethany Formation function as a leaky confining layer that separates the Columbia aquifer from the underlying confined aquifers. The thickness of the Columbia aquifer is consistent with the predicted thickness maps of Andres and Klingbeil (2006). Data evaluated by Andres and Klingbeil (2006) show that the muddy beds at the top of the Bethany Formation are not laterally continuous a few thousand feet west or east of HLSP, indicating the potential for the vertical movement of water between the Columbia and deeper aquifers.

Deposits of muddy and organic-rich sediments were found in locations consistent with Chrzastowski's (1986) paleo-environmental model of the ancestral Indian River Bay. Fine-grained lagoonal and tidal creek sediments (Figs. 6c, 7a, 7b) are the dominant lithofacies within the paleo-drainage network and marsh deposits are mostly restricted to the landward fringes of the paleo-valleys. The position and configuration of the paleo-drainage network are reflected by the locations of tidal creeks and marshes in the current landscape. Seismic reflection profiling conducted in parallel with this study (Cross et al., 2013; Banaszak, 2011) imaged the lateral boundaries of the valleys and the sandy bottom sediments, but gas in the organic-rich muds and peats often precluded imaging of the bottoms of the valley features (Figs. 6b, 6c).

The composition of the Beaverdam Formation at the study site is consistent with observations made in regional (e.g., Andres and Klingbeil, 2006) and local (e.g., Tomlinson et al., 2013) studies. Overall, grain size distribution of sediments within the Beaverdam Formation are fine and become more heterogeneous from the base of the unit toward land surface. Regionally, the Beaverdam Formation slopes and thickens toward the southeast. The lowermost 50 to 70 ft of the unit are composed of medium-to coarse-sand, with common beds of gravelly sand and sandy gravel. Individual gravelly beds tend to be thin, typically less than 1 ft in thickness. Silt is a trace component of the lower Beaverdam Formation. The uppermost 15 to 35 ft of the formation are characterized by interbedded, predominately sandy beds with

variable amounts of gravel and silt; and, predominately muddy (silt/clay mixtures) beds with variable amounts of sand. In both the lower and upper sections of the Beaverdam Formation, the sandy and muddy units appear as multiple fining upward sequences.

Within the upper Beaverdam Formation, individual muddy zones range in thickness from less than 1 ft up to 10 ft. Some muddy zones were harder and more brightly colored in hues of yellow, brown, orange, and red (YR and R hues). Regionally and at HLSP, where similar muddy beds have been observed in outcrops and cores, some of these brightly colored muddy beds are frequently mottled with gley colors (G and GY hues), indicating they are paleosols. The silt fraction of the sandier beds imparts a milky or rusty appearance with the color depending on the oxidation state of iron. (Fig. 7)

Seismic reflection profiles (Figs. 6b, 6c; Cross et al., 2013; Banaszak, 2011) illustrate the generally thin Holocene bay-bottom deposits, the slightly thicker, fine-grained, organic-rich PVF sequence, the erosional unconformity between the PVF and Beaverdam Formation, and heterogeneity within the Beaverdam Formation. In general, the internal structures and bottom surfaces of gassy, organic beds in the PVF deposits are blurred by gas wipeout, although in some cases correlation of core data allows distinction between deposits of marsh peats and tidal channel silts (Fig. 6c). Reflections in the upper, muddier, and lower, more gravelly, zones of the Beaverdam Formation are visibly distinct (Figs. 6b, 6c). Reflections within the upper Beaverdam have variable amplitude, are laterally discontinuous over hundreds of feet, and generally slope eastward, although a small number of reflectors have an apparent westward dip. The amplitude, continuity, and attitude of these reflectors in the upper Beaverdam Formation are consistent with the overall regional slope and thickness trends of the unit, as well as with borehole observations of spatially discontinuous, thin, interbedded, muddy and coarse-grained beds. These observations fit the depositional models proposed by Andres and Klingbeil (2006), Ramsey (2011), Ramsey and Tomlinson (2011, 2012) Tomlinson et al. (2013) suggesting that the upper Beaverdam Formation was deposited in an estuary dominated by variable energy, cut-and-fill, tidal channel and tidal flat environments. These shallow geologic heterogeneities have hydrologic significance. Where the mud-dominated beds of the upper Beaverdam Formation are in contact with the fine-grained PVF sediments (Fig. 6c) or crop out just below the modern bay bottom (Figs. 4d-4f), they likely function as a leaky confining unit. Correlations between zones of relatively low rates of SGD and presence of muddy beds of PVF sediment and the Beaverdam Formation, and between relatively higher rates of freshened SGD with absence of muddy PVF sediment and muddy Beaverdam were demonstrated by Russoniello et al. (2013).

Reflections within the lower Beaverdam Formation are laterally continuous over thousands feet and slope gently toward the east, an observation also made by Banaszak (2011). The character of reflectors within the lower Beaverdam Formation is consistent with borehole observations of more widely encountered, uniformly coarse grained

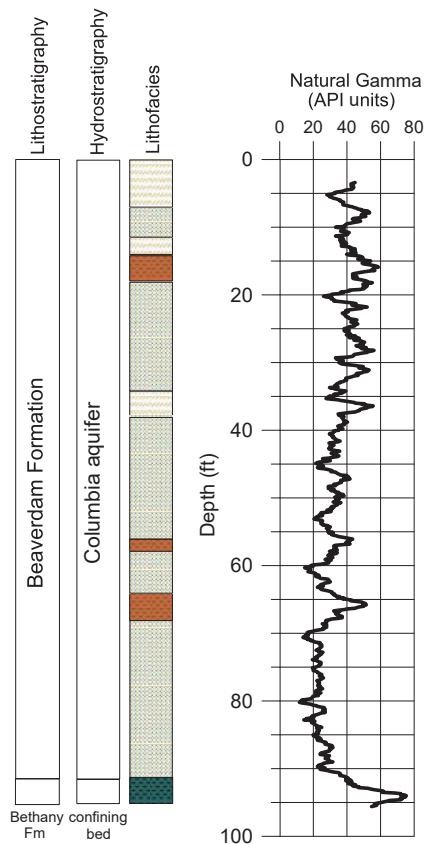


Figure 4a. Geophysical and lithological logs and interpreted litho- and hydro-stratigraphy at IN1 (Pi52-07). A key to lithofacies appears after Fig. 4f.

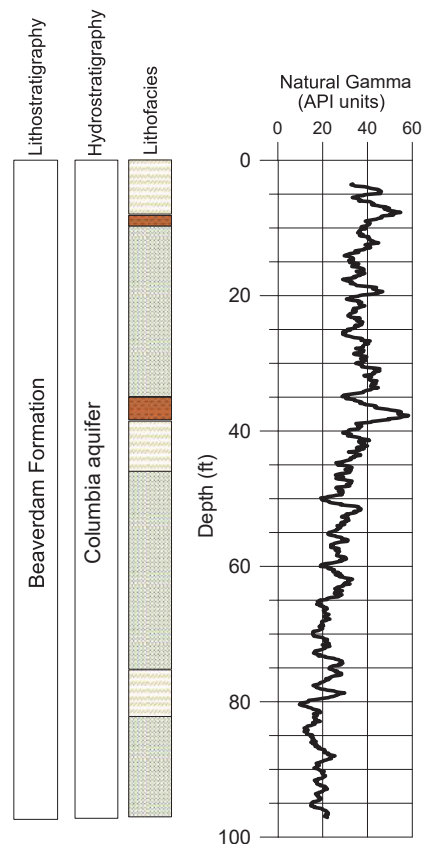


Figure 4b. Geophysical and lithological logs and interpreted litho- and hydrostratigraphy at S1 (Pi53-06). A key to lithofacies appears after Fig. 4f.

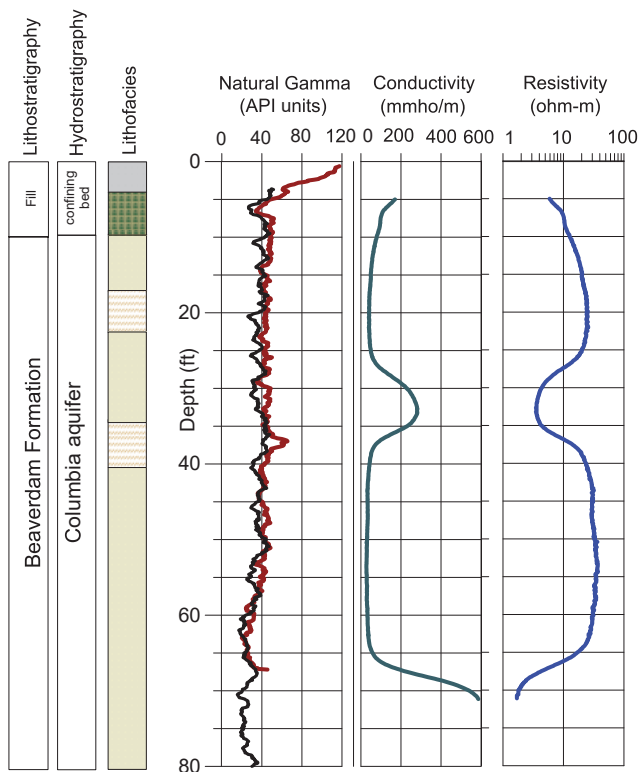


Figure 4c. Geophysical and lithologic logs and interpreted litho- and hydrostratigraphy at S4 (Pi53-10). A key to lithofacies appears after Fig. 4f.

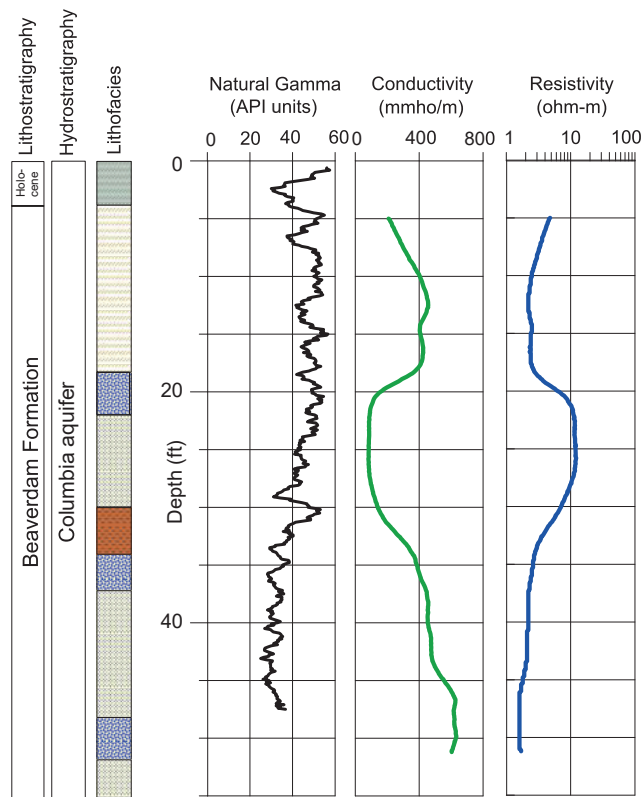


Figure 4d. Geophysical and lithological logs and interpreted litho- and hydrostratigraphy at CMT6 (Pi53-54). A key to lithofacies appears after Fig. 4f.

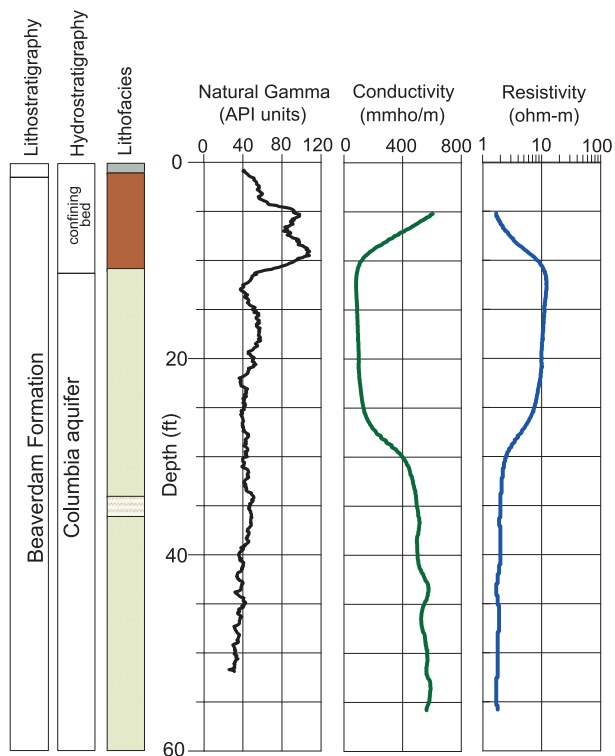


Figure 4e. Geophysical and lithological logs and interpreted litho- and hydrostratigraphy at CMT7 (Pi53-61). A key to lithofacies appears after Fig. 4f.

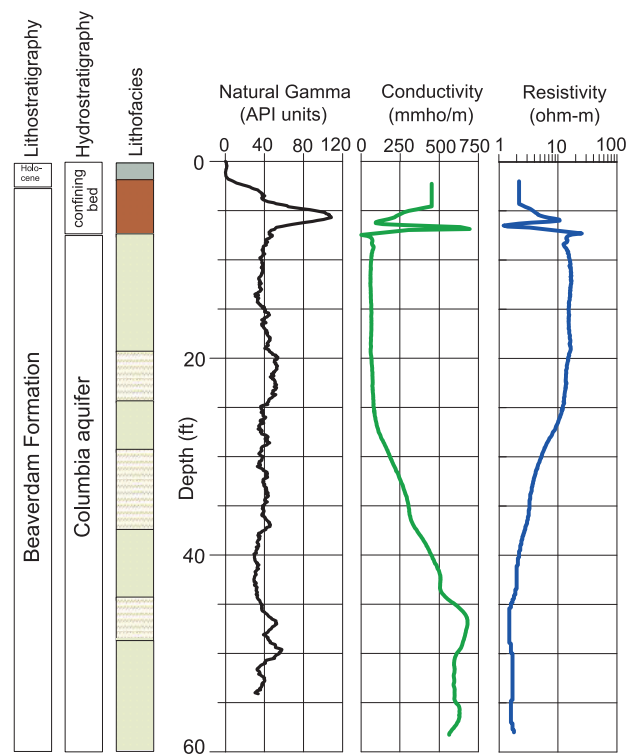
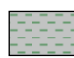


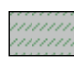
Figure 4f. Geophysical and lithological logs and interpreted litho- and hydrostratigraphy at CMT8 (Pi53-68). A key to lithofacies appears after this figure.

Key to lithofacies appearing in Figures 4a through 4f


 Fill

Holocene Lithofacies


 muddy sand to sandy mud, trace gravel and shell fragments
sub-tidal, moderate energy, bay bottom

 silty sand to sand, trace gravel and shell fragments
sub-tidal to inter-tidal, shoreline

 mud to sandy mud
tidal flat, low-energy tidal channel and bay bottom

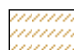
 peat and organic silt, mud and organic, organic-rich muds, trace sand
marsh, tidal flat, low-energy tidal channel

Beaverdam Formation Lithofacies


 sandy, silty, clay; clayey, sandy silt, trace gravel, mottled

 sandy gravel to gravelly sand

 sand, trace gravel and silt; gravelly sand

 silty sand to sandy clay, trace gravel

Bethany Formation Lithofacies

 sandy, silty, clay; clayey, sandy silt

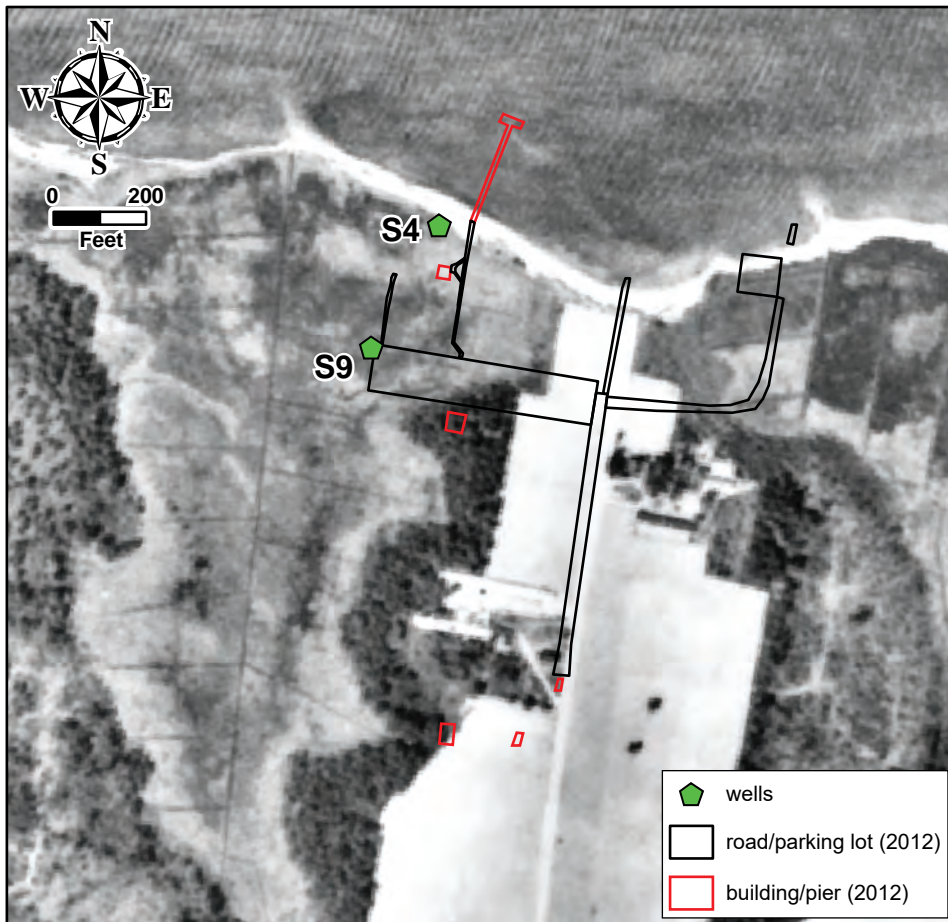


Figure 5. Interpreted 1937 aerial photograph. Note that the marsh (e.g., interpreted as darker color land cover at S9) extends under the modern parking lot and the site of well S4. Roads and structures were traced from a 2007 aerial photograph.

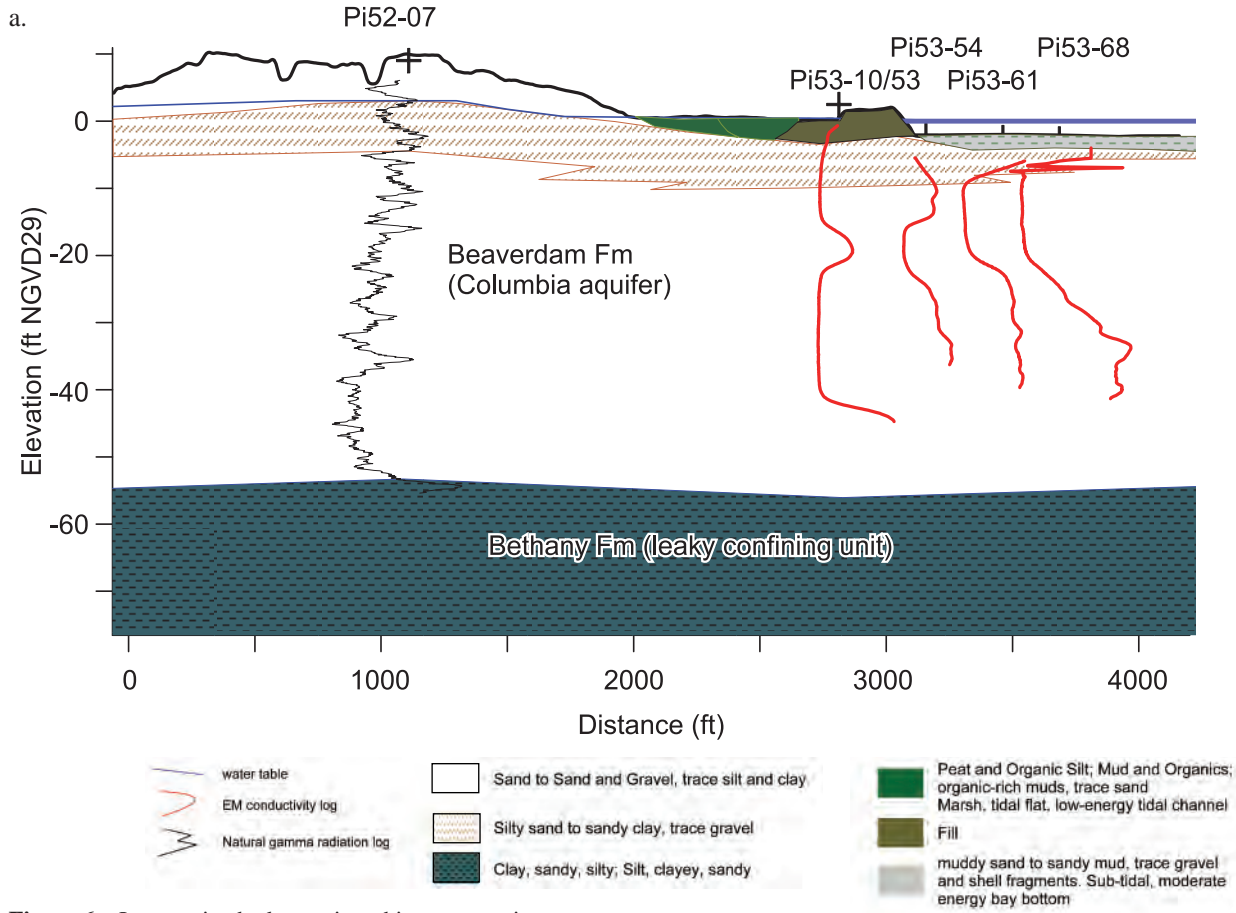
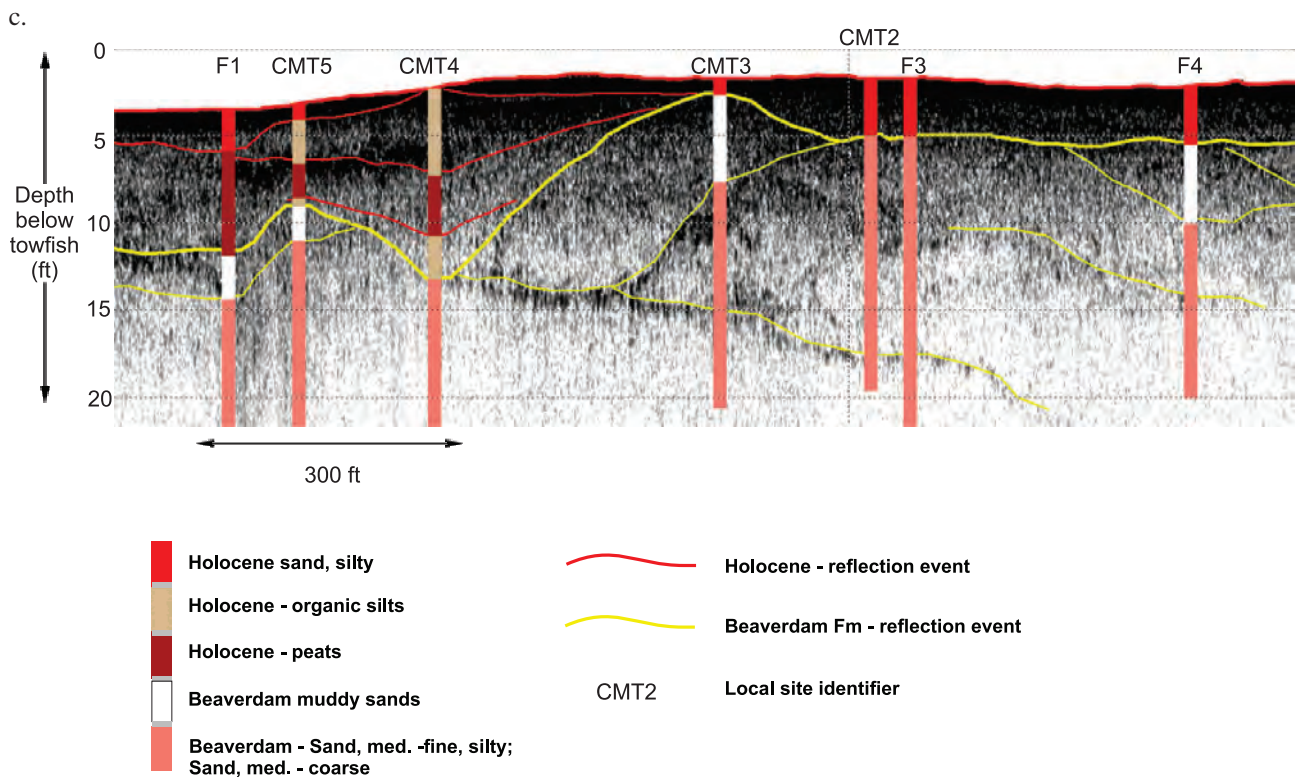
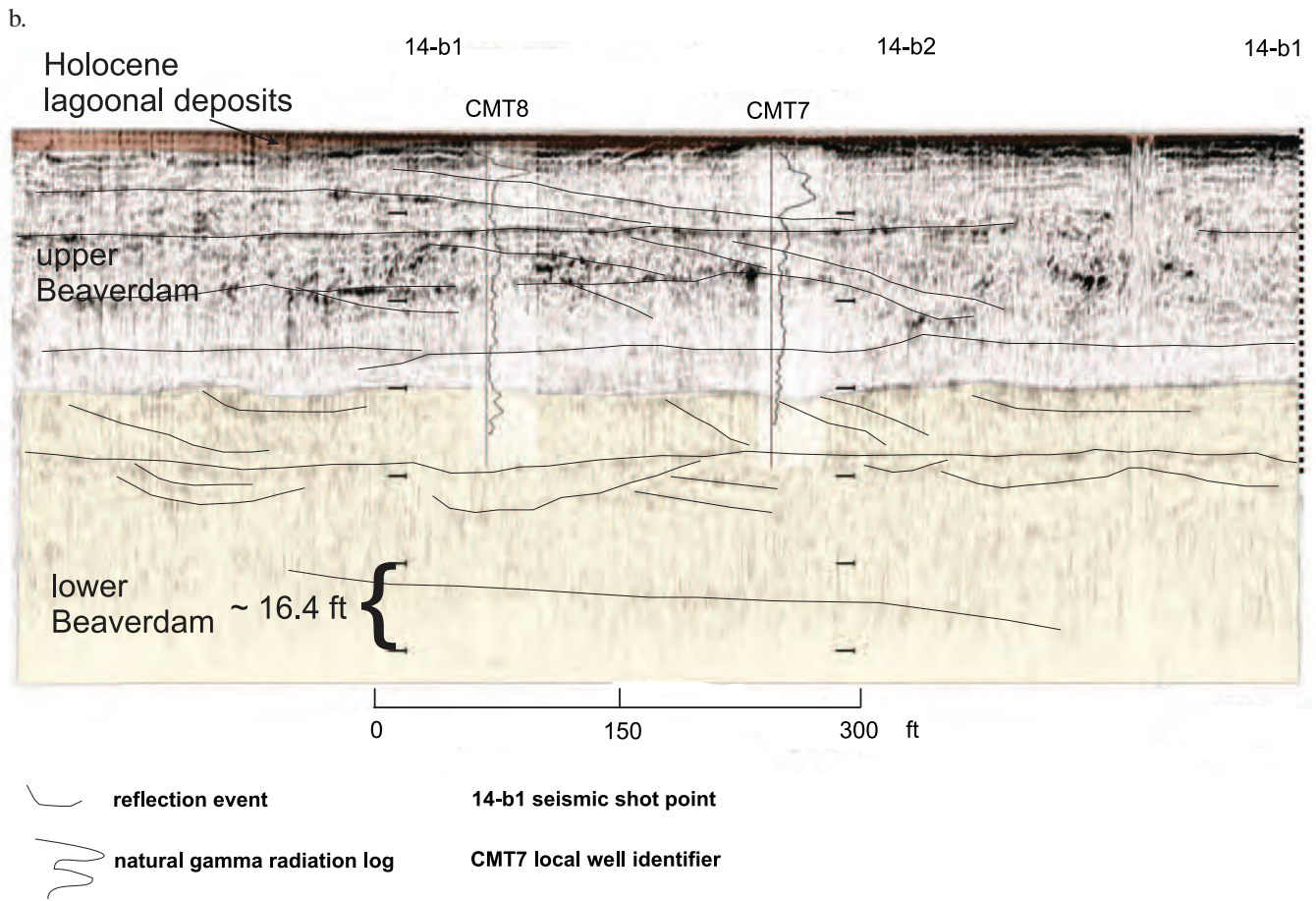


Figure 6a. Interpretive hydrostratigraphic cross section.



Figures 6b, c. Interpreted seismic reflection profiles. Well and seismic line locations are shown on Figure 2a. (b) Interpreted borehole logs (seismic data from Banaszczek, 2011). Brown shading highlights Holocene sediments, yellow shading highlights the lower Beaverdam Formation. (c) Downhole lithologic logs (seismic data from Cross et al., 2013).

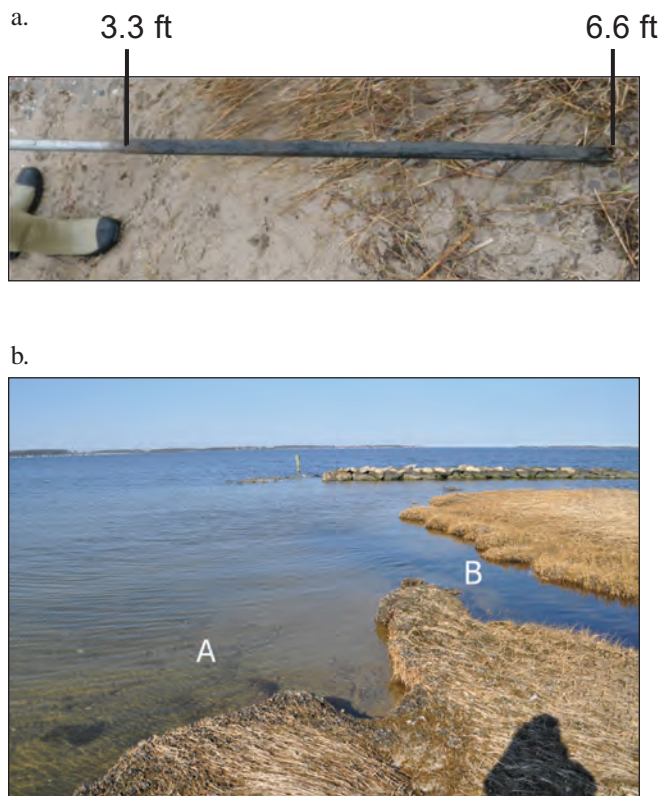


Figure 7. Core through Holocene marsh deposits, and modern marsh landscape. (a) portion of core in organic-rich Holocene marsh and tidal channel mud deposits, top and bottom of core interval are 3.3 and 6.6 ft, respectively, (b) modern marsh landscape with sandy bottom sediments visible at A, note the dark-colored marsh and tidal channel deposits exposed in a modern creek channel at B.

beds. In the context of the depositional models proposed by Andres and Klingbeil (2006), Ramsey (2011), Ramsey and Tomlinson (2011, 2012), and Tomlinson et al. (2013), the lithologic and seismic data are consistent with deposition of the sheet sands in the high-energy locations of an estuary. These coarse-grained beds limited the depths of boreholes advanced by the barge-mounted drilling system.

Hydrologic and Hydraulic Observations

K values (Table 1) measured at HLSP fall within the range observed throughout the region (Andres, 2004; Andres and Klingbeil, 2006). K values are consistent with the fining upward nature of the Beaverdam Formation and the fine-grained character of the hydraulic fill; K values in the lower Beaverdam (73–410 ft/d, $n=4$) are larger than those in the upper Beaverdam (0.81–29 ft/d, $n=4$) and hydraulic fill (2.5 ft/d, $n=2$).

The general effects of weather conditions on groundwater levels were determined from two long-term monitoring wells (wells Qe44-01 and Ng11-37 on Fig. 1) and varied from near record dry (summer 2010, 2011) to near record wet (winter 2010). This broad range of conditions is reflected in hydrographs (Fig. 8, Appendix A) from inland project wells, which show head changes of as much as 6 ft. Groundwater recharge occurs primarily from late winter to early spring and also during major summer storms, such as

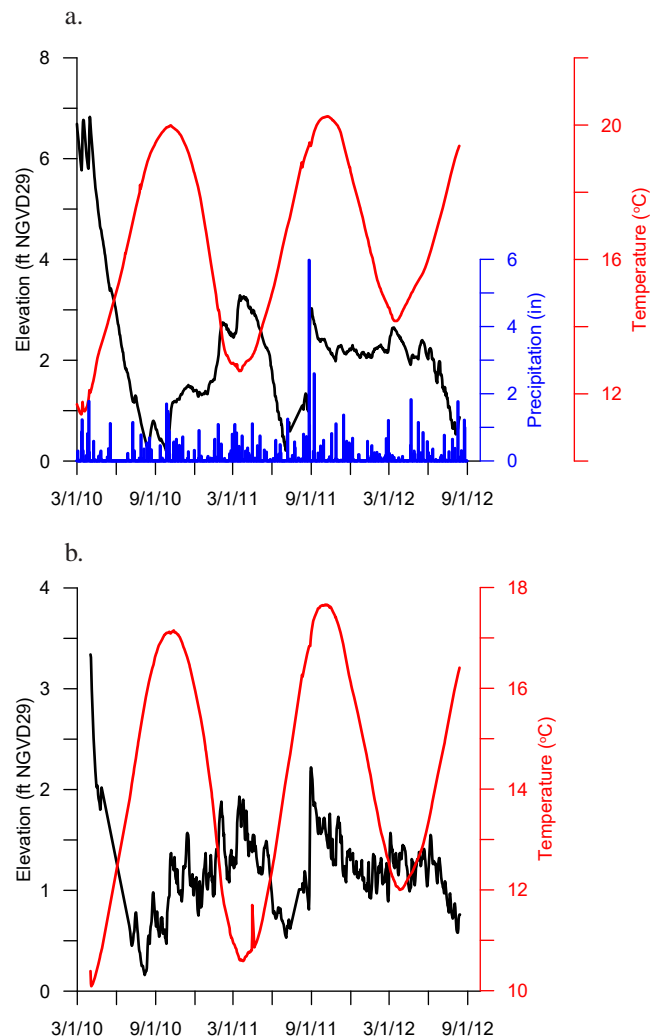


Figure 8. Groundwater levels and temperatures from selected inland wells, and precipitation at Georgetown, DE. (a) Groundwater level and temperature from well IN5 (Qi13-06), and precipitation at Georgetown, DE. (b) Groundwater level and temperature from well IN1 (Pi52-07). Note the changes from near record high groundwater elevations in winter 2010 to near record low groundwater elevations in summer 2011, and the rise in water elevation associated with the Hurricane Irene precipitation event in August 2011.

Hurricane Irene in 2011, and is coincident with increased temperatures and water elevations (Fig. 8). Annual ranges of daily mean water levels are much smaller in nearshore and offshore wells compared to inland wells (Fig. 9, Appendix A) while monthly ranges of daily mean water levels are greater in nearshore and offshore wells than in inland wells indicating that the influence of seasonal and tidal effects on water levels vary by position relative to the shoreline.

Wells finished at multiple depths in the same location, known as well clusters, were installed at three locations. Together with lithologic and hydraulic data, head differences between wells in a cluster reveal the potential for water to flow vertically at that location. By convention, positive head differences and gradients occur when heads are greater at shallower depths than at deeper depths, and indicate the potential for downward flow of water. The vertical flux of water is dependent on the hydraulic characteristics of the

Table 1. Hydraulic conductivity (K) determined by slug-test methods in project wells. Data analysis conducted in AquiferTest Pro (SWS). Note: BR – Bouwer and Rice, BU – Butler high K, Tbd – Beaverdam Formation, l – lower, u – upper.

DGS Identifier	Local Identifier	K (ft/d)	Analysis Method	Unit
Pi52-07	IN1	12	BR	Tbd u
Pi52-08	IN2	73	BR	Tbd l
Pi52-09	IN3	150	BR	Tbd l
Pi53-06	S1	0.81	BR	Tbd u
Pi53-07	S2	29	BR	Tbd u
Pi53-08	S3	100	BR	Tbd l
Pi53-10	S4	0.49	BR	fill
Pi53-12	IN4	9.8	BR	Tbd u
Pi53-13	IN5	4	BR	fill
Pi53-30	S5	3.9	BR	Tbd u
Pi53-53	S6	410	BU	Tbd l

materials, such as the K and the degree of vertical anisotropy of K (e.g., $K_x:K_z$). Although the vertical anisotropy of K, with $K_x > K_z$ is a common characteristic of sedimentary deposits, it is very difficult to collect the data needed to determine this ratio (Freeze and Cherry, 1979).

In this study, the mean and median vertical head differences for clusters 1 and 3 were very small (<0.05 ft), close to the accuracy of the instrumentation. The average head differences at cluster 2 were slightly larger (0.2 ft), and the distribution was skewed toward downward flow (median ~ 0.07 ft). An assessment of the direction and number of consecutive days (i.e., duration) of head differences (Table 2) revealed more complex relationships between cluster location, depth, and the characteristics of positive and negative head differences. The maximum durations of negative or positive head differences ranged from a few weeks to a few months, indicating the periods for which there is a significant potential for vertical flux in the aquifer. However, nega-

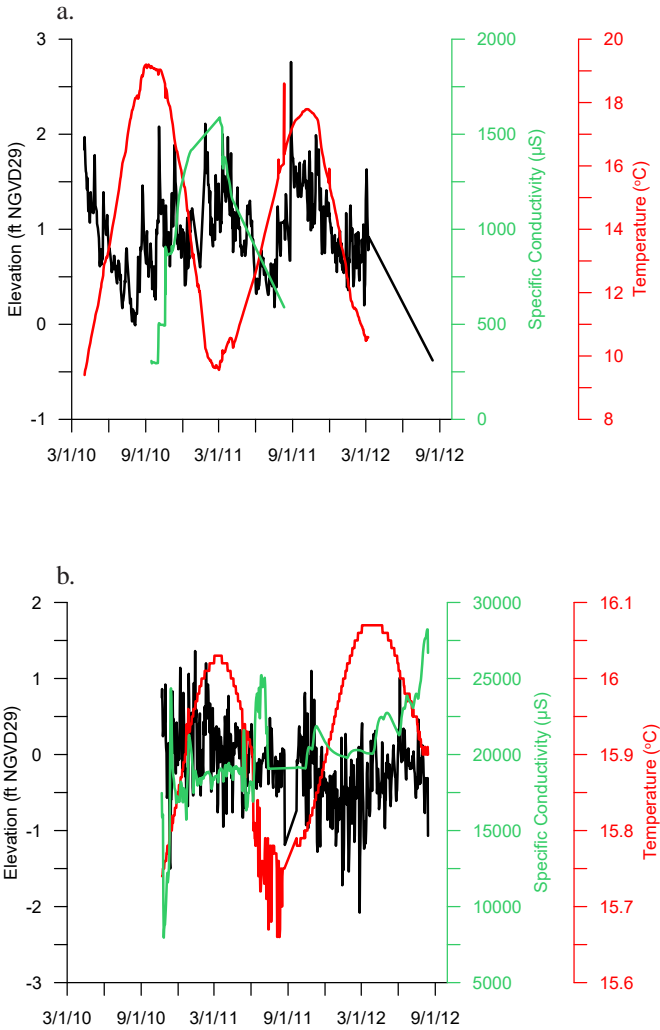


Figure 9. Groundwater levels, temperatures, and specific conductivity from selected on-land, near shore and bay wells. (a) Groundwater levels, temperature, and specific conductivity, from well S1 (Pi53-06), (b) Groundwater levels, temperature, and specific conductivity from well F3 (Pi53-14). Hurricane Irene precipitation event in August 2011.

	Cluster 1 s-m difference duration (days)	Cluster 1 s-d difference duration (days)	Cluster 2 s-m difference duration (days)	Cluster 3 s-m difference duration (days)	Cluster 3 s-d difference duration (days)
minimum	-91	-23	-18	-123	-119
5th percentile	-17.9	-6.35	-9.9	-110.5	-70.95
25th percentile	-2	-2	-3	-48	-2.25
median	0	1	-1	-1	0.5
mean	-0.50	1.11	1.27	-16.82	-2.62
75th percentile	3	3	2	1	3.25
95th percentile	15.15	13.05	7.7	55.5	22.1
maximum	48	23	98	101	52
standard deviation	15.73	6.25	14.74	56.27	24.31
# of periods	94	114	63	11	42
# of days	783	511	4.05	414	486

Table 2. Vertical gradient data. Well cluster locations shown in Fig. 2b. Notes: s-shallow, m-medium, d-deep. Well data in Appendix A. Negative values indicate upward directed gradient.

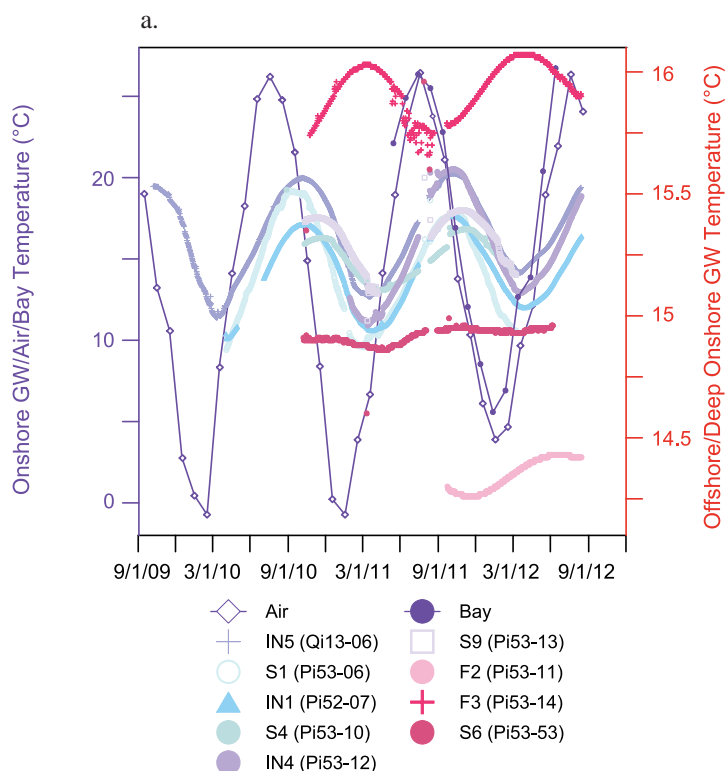
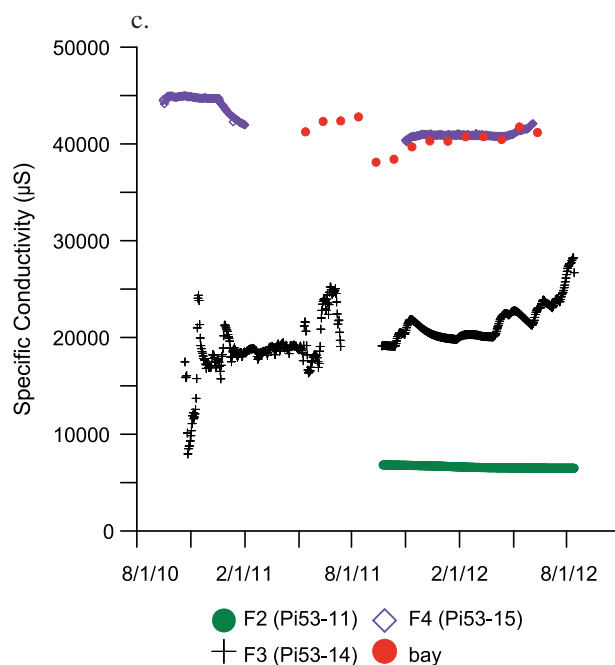
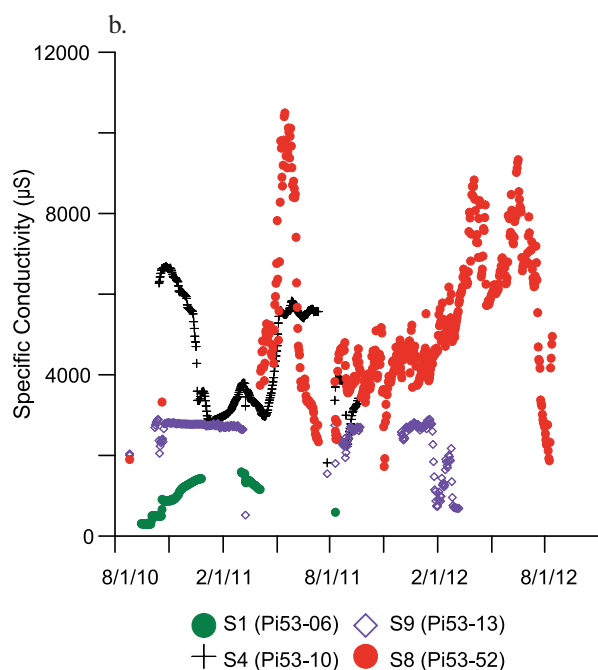


Figure 10. Comparison of groundwater temperature and specific conductivity between inland (IN5-Qi13-06, IN1-Pi52-07, IN4-Pi53-12, shoreline (S1-Pi53-06, S4-Pi53-10, S9-Pi53-13, S8-Pi53-52), and offshore wells (F2-Pi53-11, F3-Pi53-14). (a) temperature; (b) specific conductivity; (c) specific conductivity in offshore wells and monthly mean bay water.



tive or positive head differences tended to be short lived (< 3 days) at clusters 1 and 2, and at the shallow and deep pair of wells at cluster 3, suggesting that there are long periods when there is little potential for vertical flow. However, the more frequent longer periods of negative head differences between the shallow and medium depth pair of wells at cluster 3 indicate that there is more potential for upward flow between these two wells.

The temperature of air and of recharging groundwater impart a signal to shallow groundwater (Figs. 8, 9, 10) that is seen as a 4 to 7 °C difference between the warm summers and cool winters. All wells but SI (Pi53-06) also show a warming

trend between 2010 and 2011. These temperature signals are similar to those observed in other shallow wells in Delaware (DGS internal database). Wells screened in hydraulic fill show smaller temperature ranges than other shallow wells (Appendix A, S4-Pi53-10, S9-Pi53-13), indicating that the temperature range has been muted by longer travel time of water through the aquifer. Groundwater at depth on land (Fig. 9, S6-Pi53-53), and at offshore locations (Fig. 9, 10, Appendix B; In3-Pi53-09, F2-Pi53-11, F3-Pi53-14), showed the smallest temperature ranges. Average monthly bay and air temperatures (Fig. 10) have a much larger range than groundwater in on- and offshore locations.

Table 3. Timing of temperature maxima and minima. Maximum and minimum offset values in days and represent difference between offshore well Pi53-14 and other wells in table. Note: s – shallow, d – deep.

DGS Identifier	Maximum Year 1 Date	Maximum Year 2 Date	Minimum Year 1 Date	Minimum Year 2 Date	Maximum Year 1 Offset	Maximum Year 2 Offset	Minimum Year 1 Offset	Minimum Year 2 Offset	Local Identifier
Qi13-06	09/16/10	09/20/11	03/04/11	03/04/12	169	174	154	152	IN5
Pi53-06	08/26/10	10/03/11	02/06/11	02/14/12	190	161	180	171	S1
Pi53-13	10/20/10	10/15/11	03/20/11	--	135	149	138	--	S9
Pi53-53	10/08/10	09/29/11	04/13/11	03/15/12	147	165	114	141	S6
Pi53-14	03/04/11	03/12/12	08/05/11	08/03/12	--	--	--	--	F3

In previous studies in Delaware (Andres and Sims, 2013) and elsewhere (e.g., Freeze and Cherry, 1979; Anderson, 2005) groundwater temperatures and temperature fluctuations have been used to identify recharge periods, degree of aquifer confinement, and to trace movement of water masses. Throughout Delaware, the seasonal atmospheric temperature range is greater than temperature ranges observed in shallow soils and groundwater, and the atmospheric temperature maxima and minima occur one to two months prior to their appearance in soils and groundwater (Smerdon et al., 2004, 2006). The lower temperature range of groundwater versus the atmosphere likely results from the moderating influence of the porous matrix and thermal inertia of saturated porous media.

At HLSP, a smaller range of water temperature variations is observed at depth in offshore wells compared to onshore wells. The timing of the annual maximum and minimum temperatures is offset by five to six months between the onshore shallow and deep groundwater onshore and offshore, and between deep groundwater onshore and offshore (Table 3). Deep groundwater onshore (S6-Pi53-53) has maximum and minimum temperatures with similar timing to shallow groundwater but with a smaller temperature range. The inter-annual warming observed between 2010 and 2011 in shallow onshore groundwater is also observed in offshore groundwater at well F3-Pi53-14.

The possible reasons for the offset of annual maximum and minimum temperatures and the smaller intra-annual temperature variations between shallow and deep wells include the following: conductive heating of the aquifer downward from the bay or land surface; conductive heating of the well water and casing; advection of warm water from onshore to offshore; and advection of warm bay water downward into the aquifer. Given the similar geological and well construction materials, the conductive transfer of heat from warm summer air or bay water downward into the aquifer should result in similar temperatures between the onshore and offshore locations. Conductive heat transfer should also impart a time lag between maximum and minimum temperatures in shallow and deep groundwater. The fact that the expected time lag is not observed indicates that advective flux of groundwater, perhaps associated with saline recirculation along the freshwater-saltwater interface, as suggested by Bohlke and Krantz (2003), is influencing groundwater temperatures. Additional detailed assessment of groundwater flow using simulations is necessary to understand the processes and factors that control groundwater and temperature flux.

Tidal Effects

Indian River Bay tides cause groundwater levels to fluctuate in wells located on land and in the bay. These fluctuations could be caused by the loading and unloading of bay water, which changes the weight on the aquifer, and by movement of water between the bay and the aquifer (Freeze and Cherry, 1979). The first mechanism is most significant in confined or semi-confined aquifers but does not occur in unconfined aquifers. The second mechanism is most significant in unconfined aquifers. High frequency, sensor-based measurements indicate both responses in this region. Well S9-Pi53-13 (Fig. 11a) shows similar responses of head, specific conductivity, and temperature to increased tidal height, indicating the movement of more saline, warmer surface water into the aquifer. Well S4-Pi53-10 (Fig. 11b) shows similar responses in head and tide height, but the lack of response in specific conductivity and temperature are inconsistent with movement of saline surface water into this well and indicates that the aquifer at this well is confined.

The magnitude of water-level fluctuations due to tides is commonly expressed as tidal efficiency (TE), which is calculated as the ratio of tidal amplitude in a well to the tidal amplitude of the tidal body (Freeze and Cherry, 1979). TE is greatest in wells finished in the bay (Table 4), where the loading effect is greatest, and tends to decrease with increasing distance from the shoreline (Freeze and Cherry, 1979; Gregg, 1966; Serfes, 1991). The vertical stratification of aquifer hydraulic properties and consequent increase in aquifer confinement with depth observed at this site should also lead to increasing TE with depth. However, these trends are not consistently observed at this site. For example, TE at a depth of 45 ft at well cluster 1 (IN2-Pi52-08), where no confining bed was observed, is larger than TE in shallower wells located close to the shoreline (S1-Pi53-06, IN4-Pi53-12, S7-Pi53-51, and S8-Pi53-52). TE is greater in the middle of the aquifer (IN2-Pi52-08) and decreases toward both the water table (IN1-Pi52-07) and the base of the aquifer (IN3-Pi52-09). A clear identification of the mechanisms responsible for these observations at IN2-Pi52-08 is not possible from the available data. The complex spatial heterogeneity observed in the Beaverdam Formation is the most likely cause. The higher TE observed in S1-Pi53-06, completed in hydraulic fill, indicates that fine-grained sediments create less leaky confining conditions at this well compared to wells constructed at similar depths at similar distances from the bay and marsh (S1-Pi53-06, S7-Pi53-51, S8-Pi53-52).

Table 4. Tidal efficiency of wells.

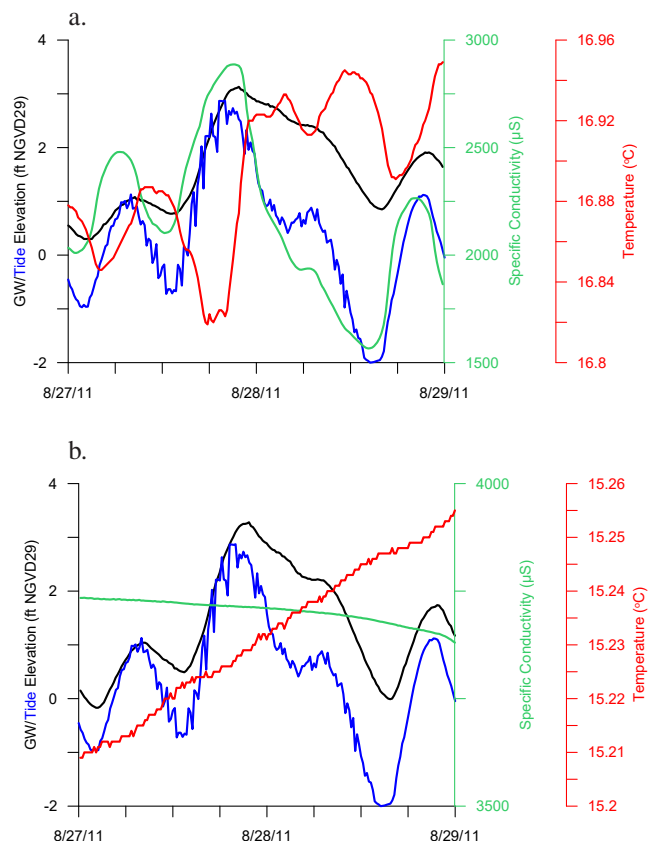
DGS Identifier	Local Identifier	Hydrologic Setting	Tidal Efficiency (%)	Notes
Pi52-07	IN1	water table	2.4	cluster 1 onshore
Pi52-08	IN2	mid-aquifer	47.7	
Pi52-09	IN3	deep aquifer	17.0	
Pi53-06	S1	water table	23.7	cluster 2 onshore
Pi53-07	S2	mid-aquifer	50.8	
Pi53-10	S4	shallow conf.	64.3	cluster 3 onshore
Pi53-30	S5	mid-aquifer	51.4	
Pi53-53	S6	deep aquifer	62.9	
Pi53-12	IN4	water table	24.9	shallow onshore
Pi53-51	S7	water table	29.7	
Pi53-52	S8	water table	29.7	
Pi53-11	F2	mid-aquifer	90.2	offshore
Pi53-14	F3	mid-aquifer	82.0	

Table 5. Comparison of electrical conductivity (EC) and specific conductivity (SC) at well cluster 3 (S4-S6). SC data collected on 8/26/10 and reported Fernandez (2012). EC log collected 8/30/10. MSZ - middle saline zone; SC - specific conductivity in micro Siemens; EC - electrical conductivity in mmho/m; depth - feet below bay bottom.

Zone/Well	Depth	EC min.	EC max.	SC	Estimated SC
Pi53-10	13.5-18.5	40.6	53.9	9370	
MSZ	27-37	100.1	282.4	--	5147-17536
Pi53-30	42-47	31.2	37.2	678	
Pi53-53	68.5-73.5	398.3	586.5	36420	

Freshwater – Saltwater Interface

The results from test drilling and downhole geophysical logging are consistent with the descriptions of fresh- and salt-water beneath Indian River Bay by Krantz et al. (2004), Manheim et al. (2004), and Bratton et al. (2004). Figure 12, derived from interpretations of downhole geophysical logs, shows a plume of fresh groundwater extending under the bay offshore of Holts Landing State Park. The plume is overlain by low permeability sediments containing salty water extending downward from the bay and is underlain by salty water. This complex configuration of the freshwater-saltwater interface is consistent with dynamic, flow-driven forces rather than static, density-driven forces. The plume of fresh water extending under the bay exists because low permeability materials form a sub-bay confining unit that causes the rate of bayward fresh water flow to be greater than the rate of freshwater discharge to the bay. This interpretation of the freshwater-saltwater interface is also supported by model-based (Stegner, 1972) and field studies (Laufer, 1982) of Rehoboth Bay, groundwater salinities observed in offshore CMT wells (Fernandez, 2012), and the spatial distribution of the offshore discharge of freshened groundwater at HLSP (Russoniello, 2013). At the HLSP study site, the lithostratigraphic units forming the upper confining bed

**Figure 11.** Examples of response of head, temperature, and specific conductivity to tides. (a) Head, temperature, and specific conductivity in well S9-Pi53-13, and bay elevations. (b) Head, temperature, and specific conductivity in well S4-Pi53-10, and bay elevations

are unnamed Holocene marsh, tidal channel, and tidal flat deposits, and muddy units in the Beaverdam Formation.

Downhole conductivity (EMC) logs indicate the presence of three zones (5-20, 27-37, and >65 ft bls) of elevated EMC (>100 mmho-m) groundwater at S4, S5, and S6 (Figs. 4c, 11, Table 5), located near the fishing pier (Fig. 2). These zones are separated by zones of lower EMC, with the shallowest associated with fine-grained fill. The middle zone is within a sequence of interbedded sands and muddy sands in the upper Beaverdam Formation. The deepest zone occurs within an interval of gravelly coarse sand in the lower Beaverdam Formation. Wells were installed in the shallowest and deepest elevated EMC zones and in a zone of low EMC in sandy beds of the lower Beaverdam.

A comparison of EMC from the downhole geophysical log to the SC of samples collected one to two months after well completion and four days prior to log collection (Table 5) shows that higher EMC values are associated with higher SC values. However, EMC/SC is highly variable from well to well, indicating that lithology has a significant effect on the conductivity log. Assuming that the lithologies associated with S5-Pi53-30 and S6-Pi53-53 better represent the lithology of the high EMC zone between 27 and 37 ft bls than does the lithology of the fill material around S4-Pi53-10, the EMC/SC from well S6-Pi53-53 appears to produce the most reasonable estimate of maximum SC (17,536 µS) for the high EMC zone between about 27 and 37 ft bls. Using the standard approximation for conversion of conductivity to salinity

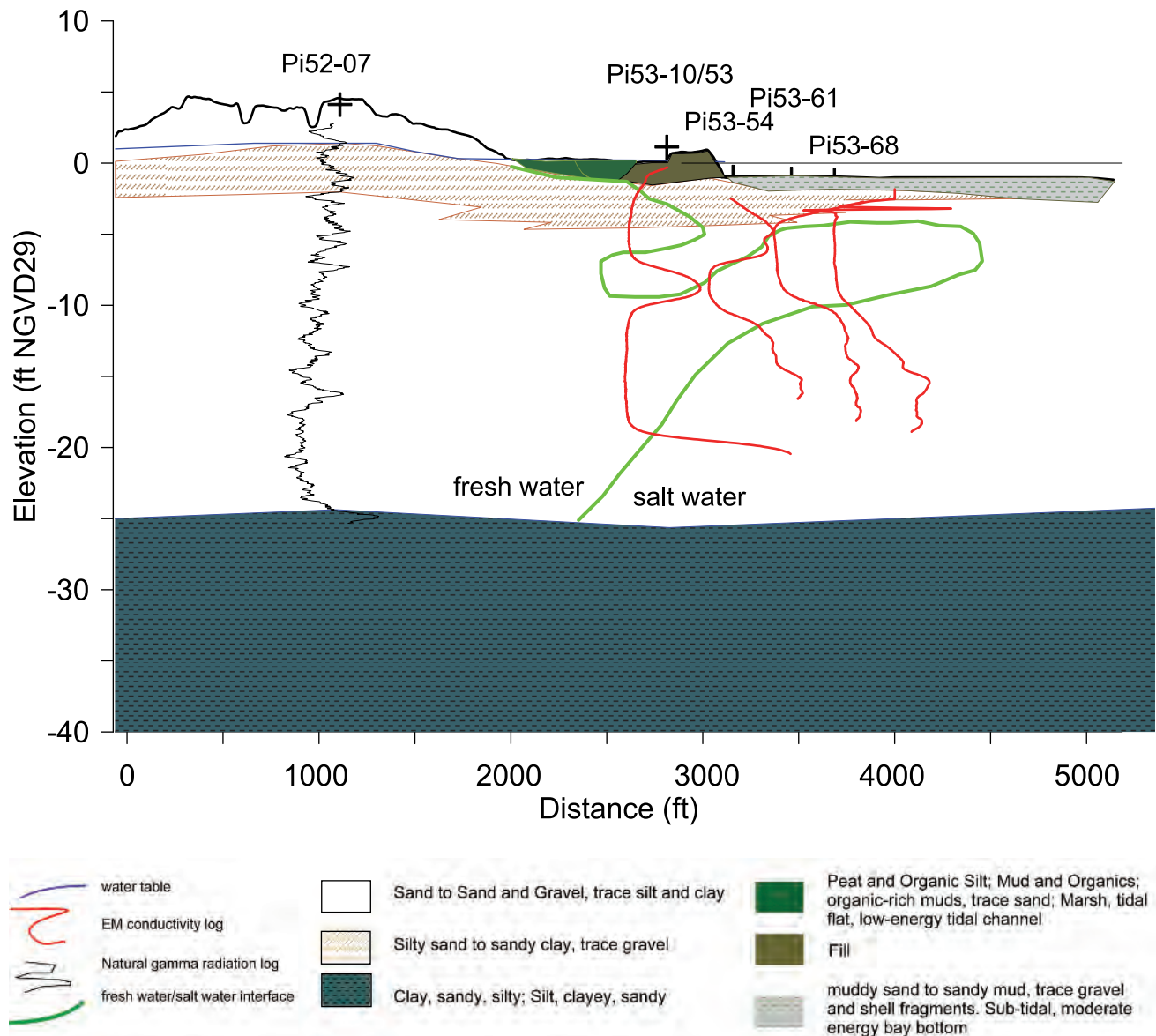


Figure 12. Interpretive cross-sectional view of freshwater-saltwater interface at Holts Landing State Park.

(Greenberg et al., 1998), this SC corresponds to a salinity of 10.3 ppt. With a typical groundwater temperature value (16°C), the water would have an approximate density of 1.007 g/cc (Fofonoff and Millard, 1983), which we postulate is large enough to support a freshwater-saltwater interface as shown in Figure 12. The presence of a freshwater-saltwater interface is also consistent with the observations of greater magnitude and duration of negative vertical head differences (potential for upward flow) in cluster 3 than at clusters 1 and 2.

The general southeasterly dip of beds in the Beaverdam Formation, the observed easterly dip of discontinuous reflectors in the seismic profile, and the absence of the body of saline water at intermediate depths in wells located further offshore indicate that this saline water feature is highly localized. The feature is most likely due to variations in the distribution, orientation, and composition of the muddy beds in the upper Beaverdam Formation with the groundwater flow field at the site. The available data are not adequate for predicting the geometry of the body of saline water.

One hypothesis tested in this study is that the magnitude of the bayward flux of fresh groundwater, a function of dynamic forcing by groundwater gradients, affects the position of the freshwater-saltwater interface more than static forcing by the density differences between fresh groundwater and saline bay water. Since the flux and the interface position cannot be measured directly from the well data, groundwater level, or head, differences (Figs. 13a, b) between inland (IN5-Qi13-06), nearshore (S4-Pi53-10), and offshore wells (F3-Pi53-14) are used as proxies for gradient and freshwater flux; specific conductance is used as a proxy for salinity and to infer a position relative to the freshwater and saltwater sides of the interface. Within an individual well, decreased specific conductivity over time indicates lower salinity and bayward movement of the interface, whereas increased specific conductivity indicates increased salinity and landward movement of the interface. These plots clearly show that gradients and, by extension, the bayward flux of fresh groundwater vary seasonally. Considering that

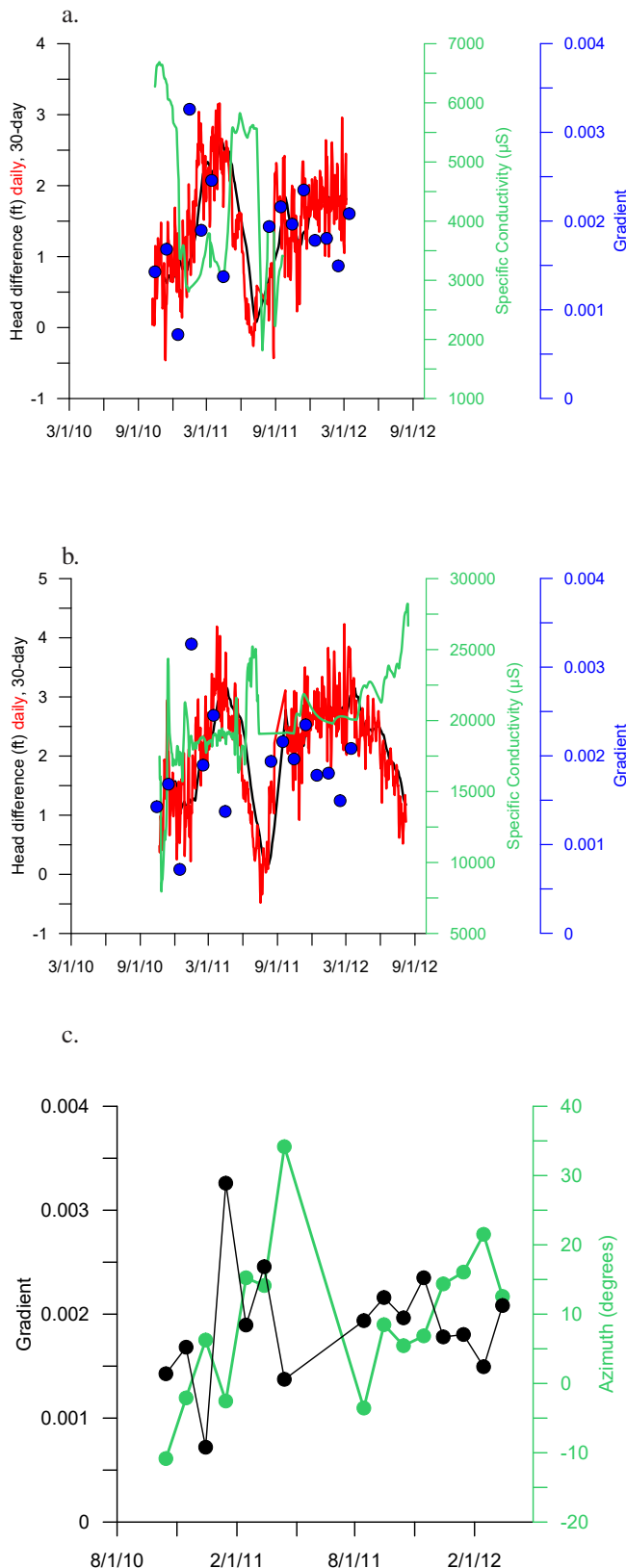


Figure 13. Comparison of hydrologic forcing and specific conductivity response. Bayward forcing is indicated by a positive head difference between inland (IN5-Qi13-06) and shoreline or inland and offshore wells. (a) Shoreline well S4-Pi53-10, (b) Offshore well F3-Pi53-14, (c) Magnitude and azimuth of gradient determined by first order fit to monthly mean groundwater elevations in wells S1-Pi53-06, S4-Pi53-10, IN4-Pi53-12, S9-Pi53-13, F3-Pi53-14, and IN5-Qi13-06.

seasonal head ranges in shoreline and offshore wells are smaller than those in inland wells, the seasonal variations in gradients are due to seasonal variation in head in inland locations and not head variations in shoreline and offshore wells. Salinity within an individual well responds within days to weeks of changes in freshwater flux with salinity rising during periods of decreased freshwater flux, and decreasing during periods of increased freshwater flux. This inverse relationship of salinity and bayward gradients over similar time scales indicates that the interface moves in response to seasonal gradient forcings rather than forcings due to static differences in density between fresh and saline water.

The site-wide gradient (Fig. 13c) determined from a first-order fit to the monthly mean groundwater elevations in wells S1-Pi53-06, S4-Pi53-10, IN4-Pi53-12, S9-Pi53-13, F3-Pi53-14, and IN5-Qi13-06 follow similar temporal trends to the head-difference plots (Figs. 13a, 13b) and average approximately 0.002, similar to values reported by Andres (1987, 2004). These gradients are generally directed slightly east of north (average 9° , Fig. 13c). The timing and magnitude of salinity variations (Figs. 13a, 13b) again appear to be dependent on the magnitude of the site-wide gradient and flux of fresh water (Figs. 13a-13c).

One subset of the above hypothesis is that the bayward of flux of groundwater varies because of seasonal or storm-related recharge, and fluctuations in the tidal height in the bay affect the position of the freshwater-saltwater interface. A 30-day, trailing moving averages of head difference computed to filter variability due to lunar tidal cycles and storms (Figs. 13a, 13b) show that the gradient changes due to climatic recharge trends are larger than gradients due to monthly lunar tidal cycles. This indicates that seasonal trends have a larger magnitude impact on the bayward flux of groundwater than do tidal cycles and storms. By extension, the bayward flux of groundwater has a larger magnitude impact on salinity and the position of the freshwater-saltwater interface than factors related to tidal cycles.

This study revealed time and magnitude thresholds of freshwater flux changes at which salinity changes by a significant percentage (Figs. 13a-13b). There is a time lag (of one to several weeks) between freshwater flux changes and salinity responses with offshore wells responding later (Fig. 13a) than onshore wells (Fig. 13b). In comparison, monthly variations in the salinity of bay water are small compared to groundwater (Fig. 10c), indicating the dominant effect of freshwater flux in the position of the freshwater-saltwater interface.

We had postulated that the position of the freshwater-saltwater interface would respond to extreme weather events and higher than normal storm tides, which could cause a vertical intrusion of saline water from the land surface or the landward movement of the interface. When Hurricane Irene (August 27-29, 2011) brought both high tides (Fig. 11) and significant rainfall (Fig. 8), head and temperature both increased in inland wells in response to the storm. Salinity increased in one shoreline well (Fig. 12a), indicating that tidal elevations were great enough to move saline water into the aquifer locally. In contrast, salinity in a shoreline well

(S8-Pi53-52, Fig. 14) decreased, and in addition, the character of tidal periodicity in salinity and temperature patterns was muted, indicating that recharge by precipitation, which increased heads by more than one foot, offset the effects of any migration of saline bay water into the aquifer.

Saline intrusion was observed during some high tides not associated with precipitation events. For example in early June, 2012, two successive high tides flooded the ground around several of the shallow shoreline wells. During this period, at well S8-Pi53-52 (Fig. 15a), groundwater elevations increased approximately 0.5 ft, and salinity increased by 10- to 20-percent of pre-event values, indicating that there was some movement of saline water into the aquifer. This well exhibited opposite trends in salinity during Hurricane Irene (Fig. 11) indicating that recharge of precipitation increased the flux of fresh groundwater enough to stop vertical infiltration of saline baywater that flooded land at the well head. In contrast, salinity and temperature in offshore well F3-Pi53-14 (Fig. 15b) did not exhibit tidal periodicity during the June 2012 period. The upward trend in salinity was part of a longer trend most likely due to the decreasing bayward flux of fresh water (Figs. 13a-13c).

CONCLUSIONS

Groundwater monitoring in and around Holts Landing State Park between October 2009 and August 2012 was part of a larger study investigating the flux of fresh groundwater

and N and P from onshore to discharge locations in Indian River Bay. Data from test drilling, geophysical logging, geophysical surveys, and well testing were used to establish the hydrogeologic framework for the study area. At this site, the Columbia aquifer is approximately 100 ft thick and is generally unconfined, though the aquifer exhibits the characteristics of a confined aquifer in two shallow wells. The lower two-thirds of the aquifer appear to be more permeable than the upper portion. Confirming the results of previous studies, fresh groundwater extends several hundred feet under the bay. This freshwater plume is bounded on the top by low permeability sediments and saline water and on the bottom by denser saline groundwater.

Groundwater levels, temperatures, and salinities respond to climatic, seasonal, and storm-related weather patterns, as well as to tidal variations. Climatic and seasonal patterns had greater effects on groundwater than did shorter term weather and tidal events. Hurricane Irene, which brought a large amount of precipitation and flooding during high tide, did not appear to cause infiltration of saline bay water into the aquifer. Conversely, a spring tidal flooding event not associated with a storm allowed minor amounts of saline water to infiltrate into the aquifer in the shallow nearshore area.

Groundwater temperature patterns vary with distance from the bay and depth in the aquifer. Groundwater flow affects temperatures in locations beneath the bay. More work

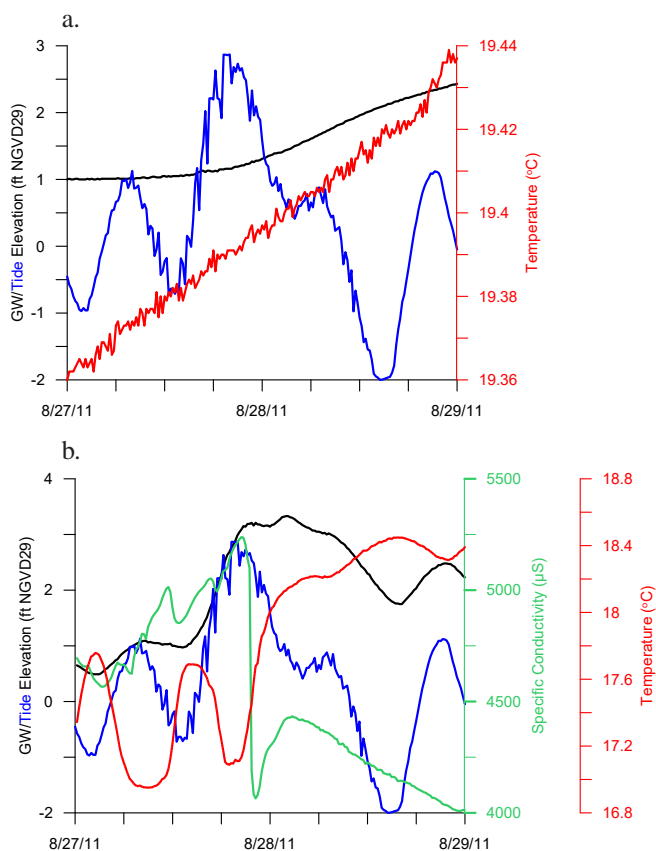


Figure 14. Head, temperature, and specific conductivity variations during Hurricane Irene at wells S8-Pi53-52 and IN5-Qi13-06, and tide elevations. (a) Groundwater head and temperature in IN5 (Qi13-06), (b) head, temperature, and specific conductivity in well S8 (Pi53-52), and tide elevations

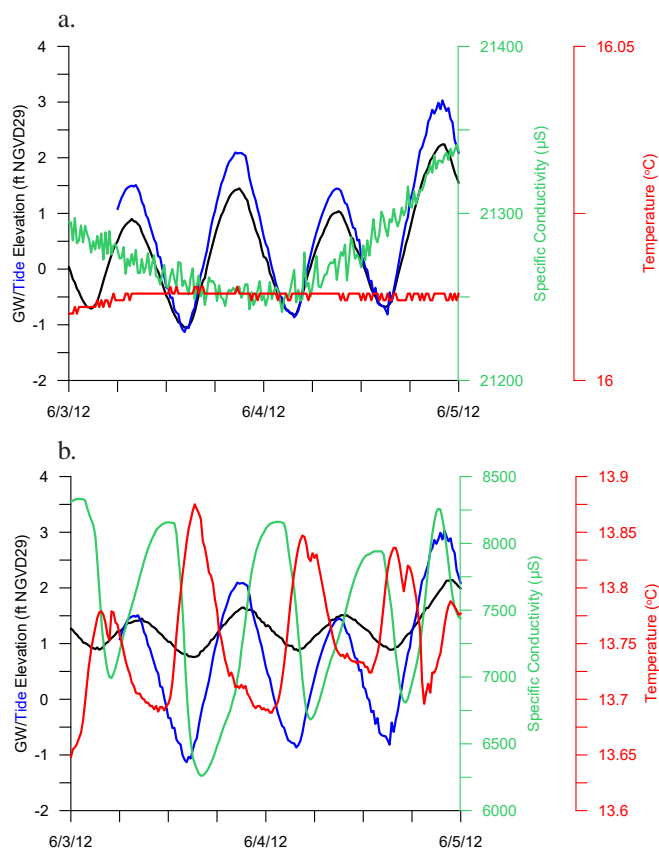


Figure 15. Head, tide height, and specific conductivity variations during a high tide event in June 2012. (a) Head, tide height, and specific conductivity in offshore well F3-Pi53-14, and tide elevation, (b) head, tide height, and specific conductivity in onshore well S8-Pi53-52, and tide elevation.

is needed to understand the relative contributions of conductive heating versus advective transport of heat with flowing groundwater. Climatic and seasonal variability in the bayward flux of fresh groundwater appears to have more of an effect on the position of the freshwater-saltwater interface than do shorter term storm and tidal events.

REFERENCES CITED

- Anderson, M. P., 2005, Heat as a ground water tracer: *Ground Water*, v. 43, p. 951-968.
- Andres, A.S., 1987, Estimate of Direct Discharge of Fresh Ground Water to Rehoboth and Indian River Bays: Delaware Geological Survey Report of Investigation No. 43, 37 p.
- Andres, A. S., 2004, Ground-water recharge mapping in Kent and Sussex counties, Delaware: Delaware Geological Survey Report of Investigations No. 66, 20 p.
- Andres, A.S. and Klingbeil, A.D., 2006, Thickness and Transmissivity of the Unconfined Aquifer of Eastern Sussex County, Delaware: Delaware Geological Survey Report of Investigation No. 70.
- Andres, A.S., and Sims, J.T., 2013, Assessing potential impacts of a wastewater rapid infiltration basin system on groundwater quality – case study in Sussex County, Delaware: *Journal of Environmental Quality*, v. 42, p. 391-404.
- Banaszak, J.F., 2011, Hydrostratigraphic framework for the surficial aquifer in the Indian River Bay, Delaware watershed: MS Thesis, Univ. of Toledo, 204 p.
- Böhlke, J.K., and D.E. Krantz. 2003. Isotope geochemistry and chronology of offshore ground water beneath Indian River Bay, Delaware: U.S. Geological Survey Water-Resources Investigations Report 03-4192, 37 p.
- Bouwer, H., 1989, The Bouwer and Rice slug test - an update: *Ground Water*, vol. 27, no. 3, p. 304-309.
- Bratton, J.F., Böhlke, J.K., Manheim, F.M., and Krantz, D.E., 2004, Submarine ground water in Delmarva Peninsula coastal bays: ages and nutrients, *Ground Water*, v. 42, p. 1021-1034.
- Brown, L. 2006, Geophysical investigation of the hydrogeologic setting of Delaware's inland bays. Ph.D. Dissertation. Department of Geology, University of Delaware, Newark.
- Butler, J. J., 1996, The design, performance, and analysis of slug tests: Boca Raton, Lewis Publishers, 252 p.
- Chrastowski, M.J., 1986, Stratigraphy and geologic history of a Holocene lagoon: Rehoboth Bay and Indian River Bay, Delaware: Ph.D. Dissertation, University of Delaware, Newark, DE, 337 p.
- Cross, V.A., Bratton, J.F., Michael, H.A., Kroeger, K.D., Green, A., and Bergeron, E., 2013, Continuous resistivity profiling and seismic-reflection data collected in April 2010 from Indian River Bay, Delaware: U.S. Geological Survey Open-File Report 2011-1039.
- Delaware Environmental Observation System, www.deos.udel.edu
- DNREC, 1998, Total Maximum Daily Load analysis for Indian River, Indian River Bay, and Rehoboth Bay, Delaware: DNREC, Dover, DE.
- Einarson, M. D., and Cherry, J. A., 2002, A new multi-level groundwater monitoring system using multichannel tubing: *Groundwater Monitoring and Remediation*, v. 22, p. 52-65.
- ESRI, 2012, ArcMap v. 10: Redlands, CA.
- Fernandez, C., 2012, Relation of the spatial and temporal distribution of water quality parameters to hydrogeology at Indian River Bay, Delaware: field observations and modeling: University of Delaware, M.S. Thesis.
- Fofonoff, N. P., and Millard, R. C., 1983, Algorithms for the computation of fundamental properties of seawater, *Unesco technical papers in marine sciences*, v. 44, p. 1-53.
- Freeze, R. A., and Cherry, J. A., 1979, *Groundwater*: Englewood Cliffs, NJ, Prentice-Hall, 604 p.
- Golden Software, 2011, *Grapher v. 9*: Golden, CO.
- Greenberg, A.E., Clesceri, L.S., and Eaton, A.D., 1998, *Standard methods for examination of water and wastewater*: American Water Works Association, 1220 p.
- Gregg, D.O., 1966, An analysis of ground-water fluctuations caused by ocean tides in Glynn County, Georgia: *Groundwater*, v. 4, p. 24-32.
- Johannes, R., 1980, The ecological significance of the submarine discharge of groundwater: *Marine Ecology-Progress Series*, v. 3, p. 365-373.
- Krantz, D.E., Manheim, F.T., Bratton, J.F., and Phelan, D.J., 2004, Hydrogeologic setting and ground-water flow beneath a section of Indian River Bay, Delaware: *Ground Water*, v. 42, p. 1035-1051.
- Lauffer, J. R., 1982, A hydrochemical study of a shallow ground-water system peripheral to Rehoboth Bay: PhD dissertation, University of Delaware, Newark, DE, 171 p.
- Manheim, F.T., Krantz, D.E., and Bratton, J.F., 2004, Studying ground water beneath Delmarva coastal bays using electrical resistivity: *Ground Water* v. 42, p. 1052-1068.
- McKenna, K.K. and Ramsey, K.W., 2002, An Evaluation of Sand Resources, Atlantic Offshore, Delaware: Delaware Geological Survey Report of Investigation No. 63, 37 p.
- Ramsey, K.W., 2011, *Geologic Map of the Fairmount and Rehoboth Beach Quadrangles*, Delaware: Delaware Geological Survey Geologic Map No. 16, scale 1:24,000.
- Ramsey, K.W. and Tomlinson, J.L., 2011, *Geologic Map of the Harbeson Quadrangle*, Delaware: Delaware Geological Survey Geologic Map No. 17, scale 1:24,000.
- _____, *Geologic Map of the Bethany Beach and Assawoman Bay Quadrangles*: Delaware Geological Survey Geologic Map No. 18, scale 1:24,000.
- Rock Color Chart Committee, 1979, *Rock-color chart*: Boulder, CO, Geological Society of America.
- Russoniello, C.J., Fernandez, C., Bratton, J.F., Banaszak, J.F., Krantz, D.E., Andres, A.S., Konikow, L.F., and Michael, H.A., 2013, Geologic effects on groundwater salinity and discharge into an estuary: *Journal of Hydrology*, v. 498, p. 1-12.

- Selman, M., and Greenhalgh, S., 2007, Eutrophication: An Overview of Status, Trends, Policies, and Strategies. World Resources Institute: Washington, DC. [Available online at http://pdf.wri.org/eutrophication_policies_actions_and_strategies.pdf].
- Serfes, M.E., 1991, Determining the mean hydraulic gradient of ground water affected by tidal fluctuations: *Ground Water* v. 29, p. 549-555.
- Slomp, C. P., van Cappellen, P., 2004, Nutrient inputs to the coastal ocean through submarine groundwater discharge; 295, p. 64-86.
- Smerdon, J. E., Pollack, H. N., Cermak, V., Enz, J. W., Kresl, M., Safanda, J., and Wehmiller, J. F., 2004, Air-ground temperature coupling and subsurface propagation of annual temperature signals: *Journal of Geophysical Research*, v. 109, D21107-D21117.
- Smerdon, J. E., Pollack, H. N., Cermak, V., Enz, J. W., Kresl, M., Safanda, J. and Wehmiller, J. F., 2006, Daily, seasonal, and annual between air and subsurface temperatures: *Journal of Geophysical Research*, v. 111, D07101.
- Stegner, S.R., 1972, Analog model study of ground-water flow in the Rehoboth Bay area, Delaware: Technical Report 12, Newark, DE, University of Delaware, College of Marine Studies, 69 p
- Sterrett, R.J., ed., 2008, *Groundwater and wells*, 3rd edition: New Brighton, MN, Johnson Screens, 812 p.
- SWS, Inc., 2011, *AquiferTest Pro v 2*: Waterloo, Ontario, Canada.
- Tomlinson, J.L., Ramsey, K.W. and Andres, A. S., 2013, *Geology of the Frankford and Selbyville Quadrangles*, Delaware: Delaware Geological Survey Geologic Map No. 19, scale 1:24,000.
- USACE, 2004, *Corpscon*, v. 6x: USACE Engineer Research and Development Center.
- US Geological Survey, 2005, *Lidar DEM for Sussex County*, Delaware.
- U.S. Geological Survey, National Water Information Service, <http://waterdata.usgs.gov/nwis>
- Vitousek P., and Aber, J., 1997, Human alteration of the global nitrogen cycle: sources and consequences: *Ecological Applications*, v. 7, p. 737-750.
- Williams, C. P., 1999, *Late Pleistocene and Holocene stratigraphy of the Delaware inner continental shelf*: Newark, Delaware, University of Delaware, unpublished M.S. Thesis, 175 p.

APPENDIX A. Attributes of wells installed at Holts Landing State Park.

IN-inland, F-offshore, S-Onshore, S-onshore near shoreline, CMT-continuous multichannel tube well, UTM-18N-North American Datum 1983, Universal Transverse Mercator, NGVD 29-National Geodetic Vertical Datum of 1929, bls-below land surface, *estimated

DGS Identifier	Permit Number	Local Identifier	EASTING (UTM18-N m)	NORTHING (UTM18-N m)	Elevation (ft NGVD 29)	Top of screen (ft bls)	Bottom of screen (ft bls)	Well Cluster Identifier
Pi53-16	231157	CMT1-1	488906.6	4271526.3	-3.2	3.9	4.2	
Pi53-17	231157	CMT1-2	488906.6	4271526.3		7.4	7.7	
Pi53-18	231157	CMT1-3	488906.6	4271526.3		10.9	11.2	
Pi53-19	231157	CMT1-4	488906.6	4271526.3		14.4	14.7	
Pi53-20	231157	CMT1-5	488906.6	4271526.3		17.9	18.2	
Pi53-21	231157	CMT1-6	488906.6	4271526.3		21.4	21.7	
Pi53-22	231157	CMT1-7	488906.6	4271526.3		24.9	25.2	
Pi53-23	231161	CMT2-1	488792	4271561.6	-3.23	2.9	3.2	
Pi53-24	231161	CMT2-2	488792	4271561.6		6.9	7.2	
Pi53-25	231161	CMT2-3	488792	4271561.6		11.9	12.2	
Pi53-26	231161	CMT2-4	488792	4271561.6		17.9	18.2	
Pi53-27	231161	CMT2-5	488792	4271561.6		24.9	25.2	
Pi53-28	231161	CMT2-6	488792	4271561.6		34.9	35.2	
Pi53-29	231161	CMT2-7	488792	4271561.6		49.9	50.2	
Pi53-31	231162	CMT3-1	488750	4271604.2		3.4	3.7	
Pi53-32	231162	CMT3-2	488750	4271604.2		11.9	12.2	
Pi53-33	231162	CMT3-3	488750	4271604.2		20.4	20.7	
Pi53-34	231162	CMT3-4	488750	4271604.2		28.9	29.2	
Pi53-35	231162	CMT3-5	488750	4271604.2		37.4	37.7	
Pi53-36	231162	CMT3-6	488750	4271604.2		45.9	46.2	
Pi53-37	231163	CMT4-1	488628	4271593.3		6.9	7.2	
Pi53-38	231163	CMT4-2	488628	4271593.3		11.9	12.2	
Pi53-39	231163	CMT4-3	488628	4271593.3		19.9	20.2	
Pi53-40	231163	CMT4-4	488628	4271593.3		27.9	28.2	
Pi53-41	231163	CMT4-5	488628	4271593.3		35.9	36.2	
Pi53-42	231163	CMT4-6	488628	4271593.3		43.9	44.2	
Pi53-43	231163	CMT4-7	488628	4271593.3		49.9	50.2	
Pi53-44	231164	CMT5-1	488578.7	4271608.1		7.9	8.2	
Pi53-45	231164	CMT5-2	488578.7	4271608.1		14.9	15.2	
Pi53-46	231164	CMT5-3	488578.7	4271608.1		21.9	22.2	
Pi53-47	231164	CMT5-4	488578.7	4271608.1		28.9	29.2	
Pi53-48	231164	CMT5-5	488578.7	4271608.1		35.9	36.2	
Pi53-49	231164	CMT5-6	488578.7	4271608.1		42.9	43.2	
Pi53-50	231164	CMT5-7	488578.7	4271608.1		49.9	50.2	
Pi53-54	231165	CMT6-1	488812.3	4271563.4	-3.23	25.9	26.2	
Pi53-55	231165	CMT6-2	488812.3	4271563.4		29.9	30.2	
Pi53-56	231165	CMT6-3	488812.3	4271563.4		33.9	34.2	
Pi53-57	231165	CMT6-4	488812.3	4271563.4		37.9	38.2	
Pi53-58	231165	CMT6-5	488812.3	4271563.4		41.9	42.2	
Pi53-59	231165	CMT6-6	488812.3	4271563.4		45.9	46.2	
Pi53-60	231165	CMT6-7	488812.3	4271563.4		50	50.5	

APPENDIX A (cont). Attributes of wells installed at Holts Landing State Park.

IN-inland, F-offshore, S-Onshore, S-onshore near shoreline, CMT-continuous multichannel tube well, UTM-18N-North American Datum 1983, Universal Transverse Mercator, NGVD 29-National Geodetic Vertical Datum of 1929, bls-below land surface, *estimated

DGS Identifier	Permit Number	Local Identifier	EASTING (UTM18-N m)	NORTHING (UTM18-N m)	Elevation (ft NGVD 29)	Top of screen (ft bls)	Bottom of screen (ft bls)	Well Cluster Identifier
Pi53-61	231166	CMT7-1	488792.1	4271654.1	-3.7	7.9	8.2	
Pi53-62	231166	CMT7-2	488792.1	4271654.1		14.9	15.2	
Pi53-63	231166	CMT7-3	488792.1	4271654.1		21.9	22.2	
Pi53-64	231166	CMT7-4	488792.1	4271654.1		28.9	29.2	
Pi53-65	231166	CMT7-5	488792.1	4271654.1		35.9	36.2	
Pi53-66	231166	CMT7-6	488792.1	4271654.1		42.9	43.2	
Pi53-67	231166	CMT7-7	488792.1	4271654.1		50	50.3	
Pi53-68	231167	CMT8-1	488777.7	4271720.7	-4	7.9	8.2	
Pi53-69	231167	CMT8-2	488777.7	4271720.7		14.9	15.2	
Pi53-70	231167	CMT8-3	488777.7	4271720.7		21.9	22.2	
Pi53-71	231167	CMT8-4	488777.7	4271720.7		28.9	29.2	
Pi53-72	231167	CMT8-5	488777.7	4271720.7		35.9	36.2	
Pi53-73	231167	CMT8-6	488777.7	4271720.7		42.9	43.2	
Pi53-74	231167	CMT8-7	488777.7	4271720.7		50	50.3	
Pi53-09	231158	F1	488571.8	4271659.9	-2.09	40.5	45.5	
Pi53-11	231156	F2	488686	4271532.2	-0.2*	50	55	
Pi53-14	231159	F3	488811.2	4271574	-2.7*	40	45	
Pi53-15	231157	F4	488908.1	4271530	-3.46	37	42	
Pi52-07	230450	IN1	488395.1	4271120.2	14.46	8.5	13.5	cluster 1-s
Pi52-08	230452	IN2	488395	4271121	14.56	42	47	cluster 1-m
Pi52-09	230454	IN3	488395	4271122	14.27	68	73	cluster 1-d
Pi53-12	231170	IN4	488898	4271363	7.9	8	13	
Qi13-06	166163	IN5	488511	4269567	12.6	9	14	
Pi53-06	230449	S1	488491	4271452	5.42	12	14	cluster 2-s
Pi53-07	230451	S2	488491	4271452	5.54	42	47	cluster 2-m
Pi53-08	230453	S3	488491	4271452	5.42	68	73	cluster 2-d
Pi53-10	231172	S4	488790.4	4271461.7	5.57	13.5	18.5	cluster 3-s
Pi53-30	231173	S5	488788	4271461.7	5.5	42	47	cluster 3-m
Pi53-53	231175	S6	488786	4271461.7	5.51	68.5	73.5	cluster 3-d
Pi53-51	231176	S7	488516.7	4271281.2	6.31	8.5	13.5	
Pi53-52	231177	S8	488432.7	4271449.3	5.32	8.5	13.5	
Pi53-13	231171	S9	488745.9	4271382	7.67	13	18	

APPENDIX B

HYDROGRAPHS, THERMOGRAPHS, AND SPECIFIC CONDUCTIVITY GRAPHS FOR SELECT WELLS

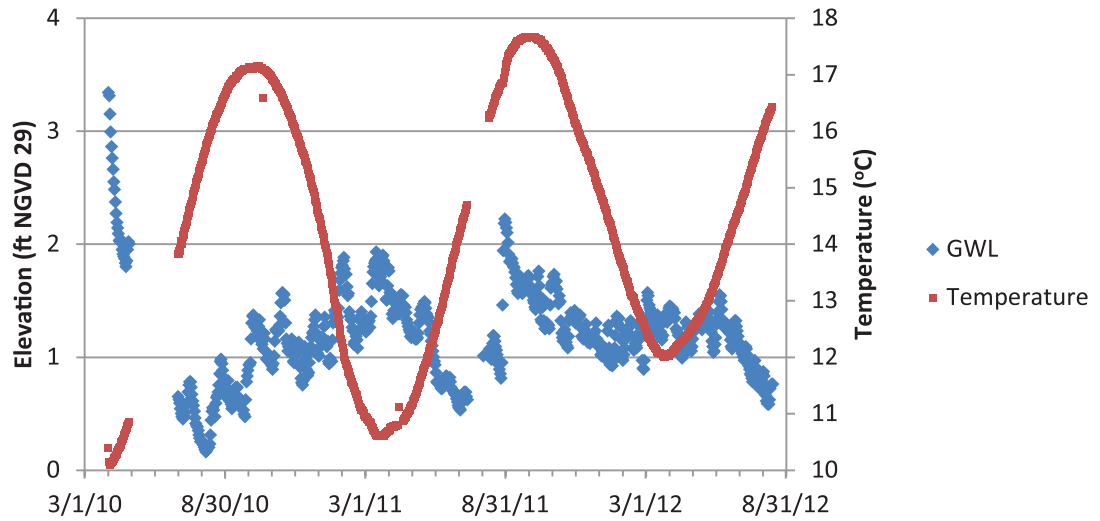


Figure B1. Hydrograph and thermograph for IN1 (Pi52-07).

NGVD29-National Geodetic Vertical Datum of 1929

GWL-groundwater level

APPENDIX B

HYDROGRAPHS, THERMOGRAPHS, AND SPECIFIC CONDUCTIVITY GRAPHS FOR SELECT WELLS

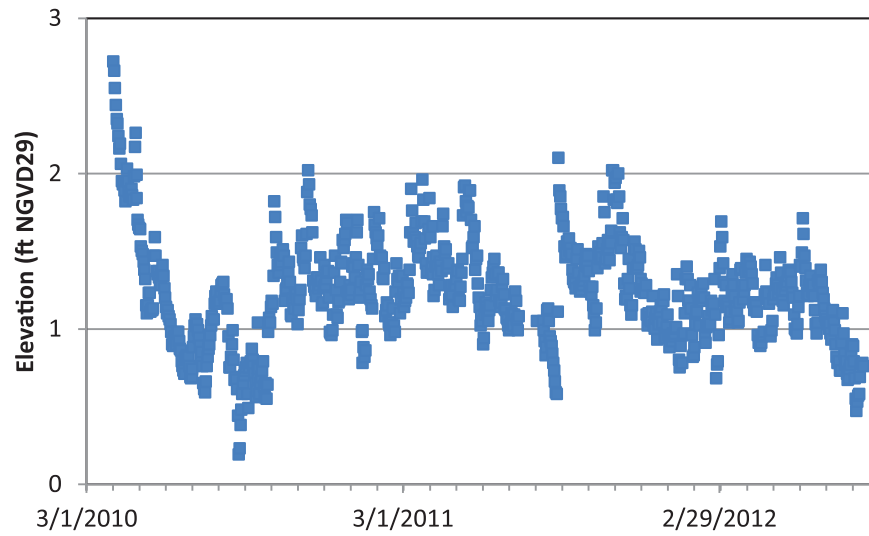


Figure B2.

Hydrograph for IN2 (Pi52-08).

NGVD29-National Geodetic Vertical Datum of 1929

APPENDIX B

HYDROGRAPHS, THERMOGRAPHS, AND SPECIFIC CONDUCTIVITY GRAPHS FOR SELECT WELLS

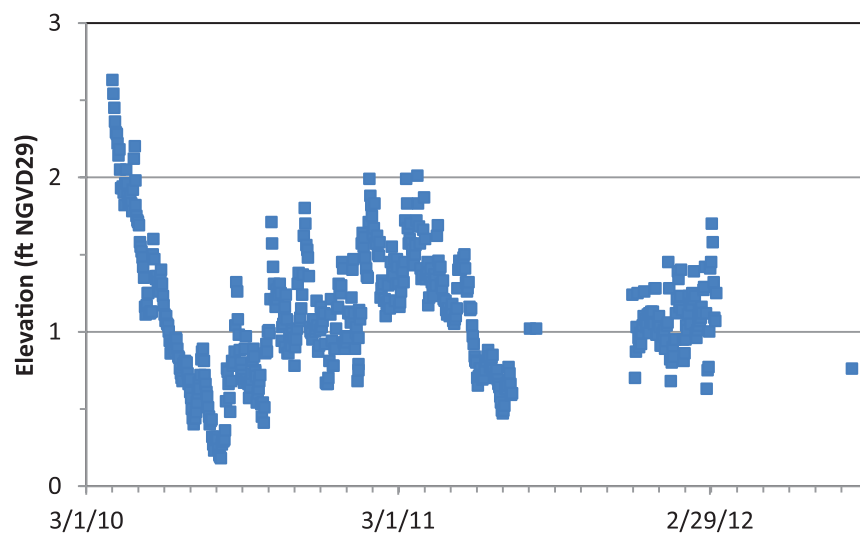


Figure B3. Hydrograph for IN3 (Pi52-09).
NGVD29-National Geodetic Vertical Datum of 1929

APPENDIX B

HYDROGRAPHS, THERMOGRAPHS, AND SPECIFIC CONDUCTIVITY GRAPHS FOR SELECT WELLS

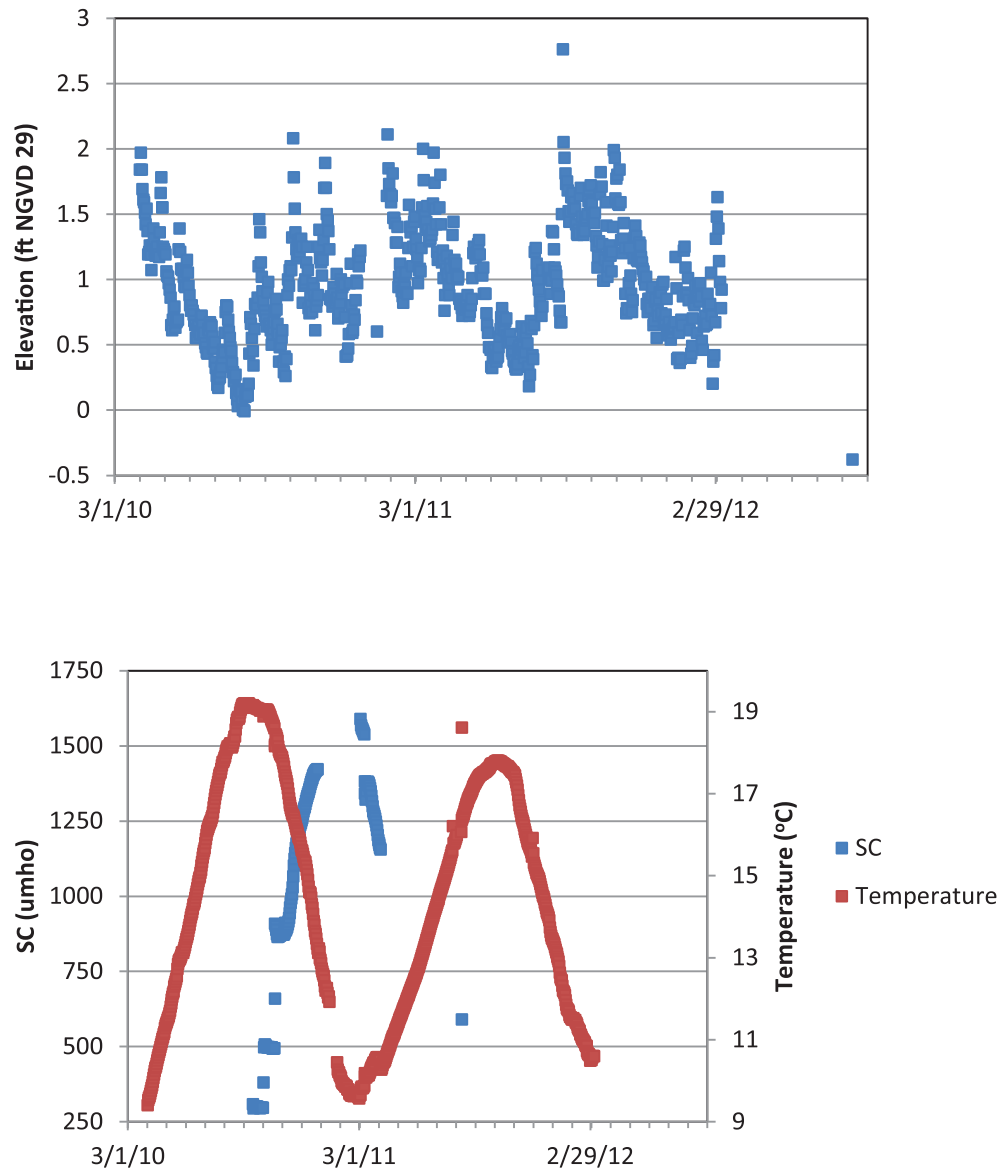


Figure B4. Hydrograph, thermograph, and specific conductivity graph for S1 (Pi53-06).
NGVD29-National Geodetic Vertical Datum of 1929
SC-specific conductivity
 μmho -micromhos

APPENDIX B

**HYDROGRAPHS, THERMOGRAPHS, AND SPECIFIC CONDUCTIVITY GRAPHS
FOR SELECT WELLS**

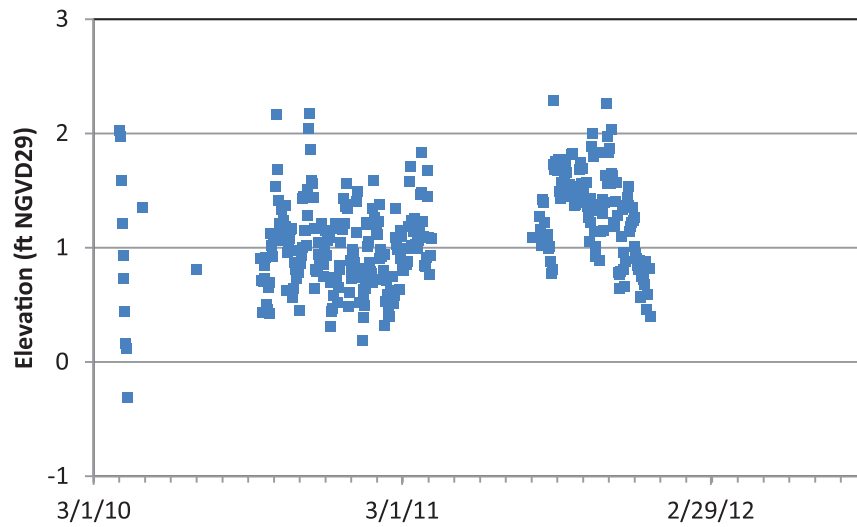


Figure B5. Hydrograph for S2 (Pi53-07).
NGVD29-National Geodetic Vertical Datum of 1929

APPENDIX B

HYDROGRAPHS, THERMOGRAPHS, AND SPECIFIC CONDUCTIVITY GRAPHS FOR SELECT WELLS

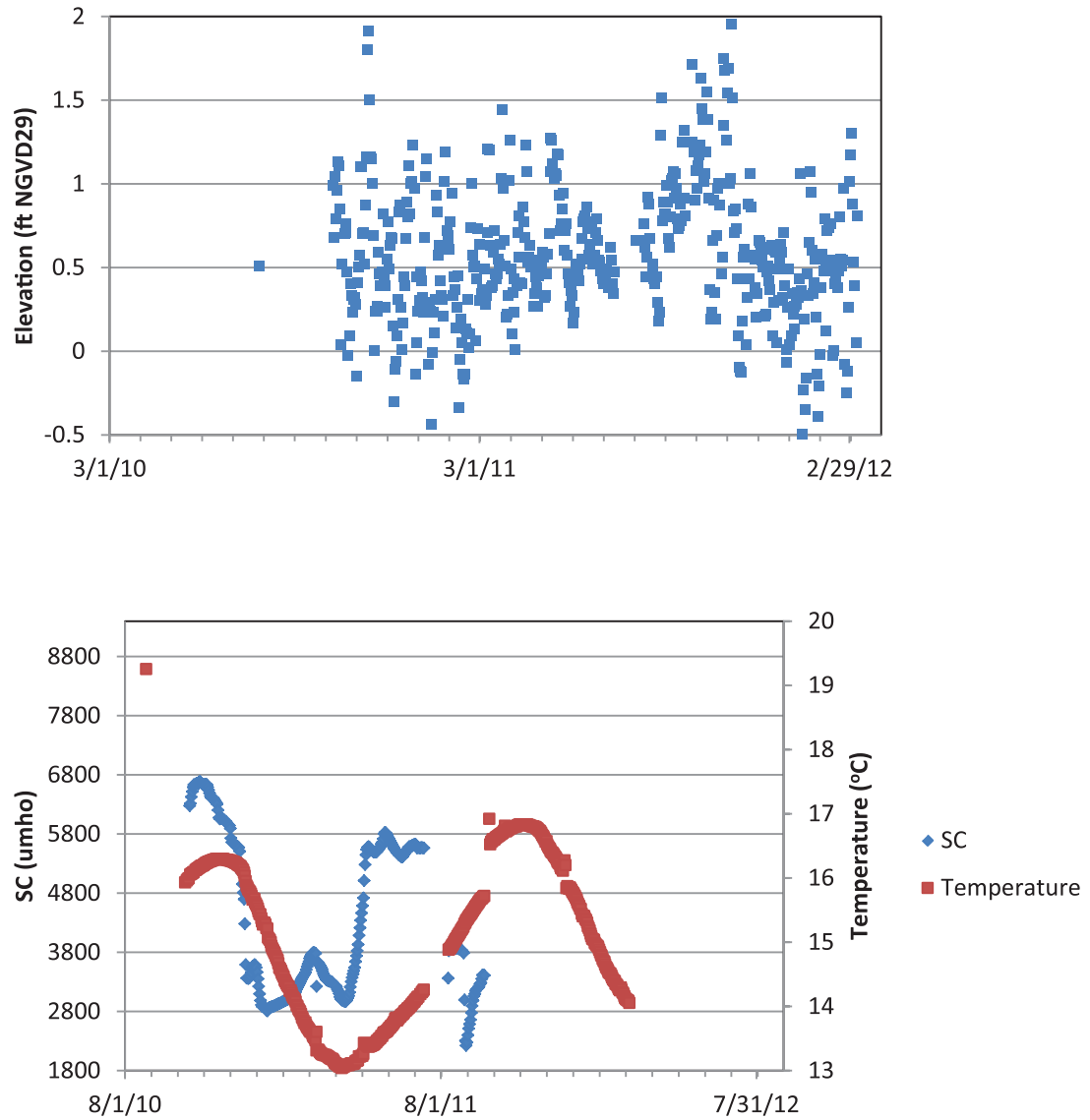


Figure B6. Hydrograph, thermograph, and specific conductivity graph for S4 (Pi53-10).
NGVD29-National Geodetic Vertical Datum of 1929
SC-specific conductivity
umho-micromhos

APPENDIX B

HYDROGRAPHS, THERMOGRAPHS, AND SPECIFIC CONDUCTIVITY GRAPHS FOR SELECT WELLS

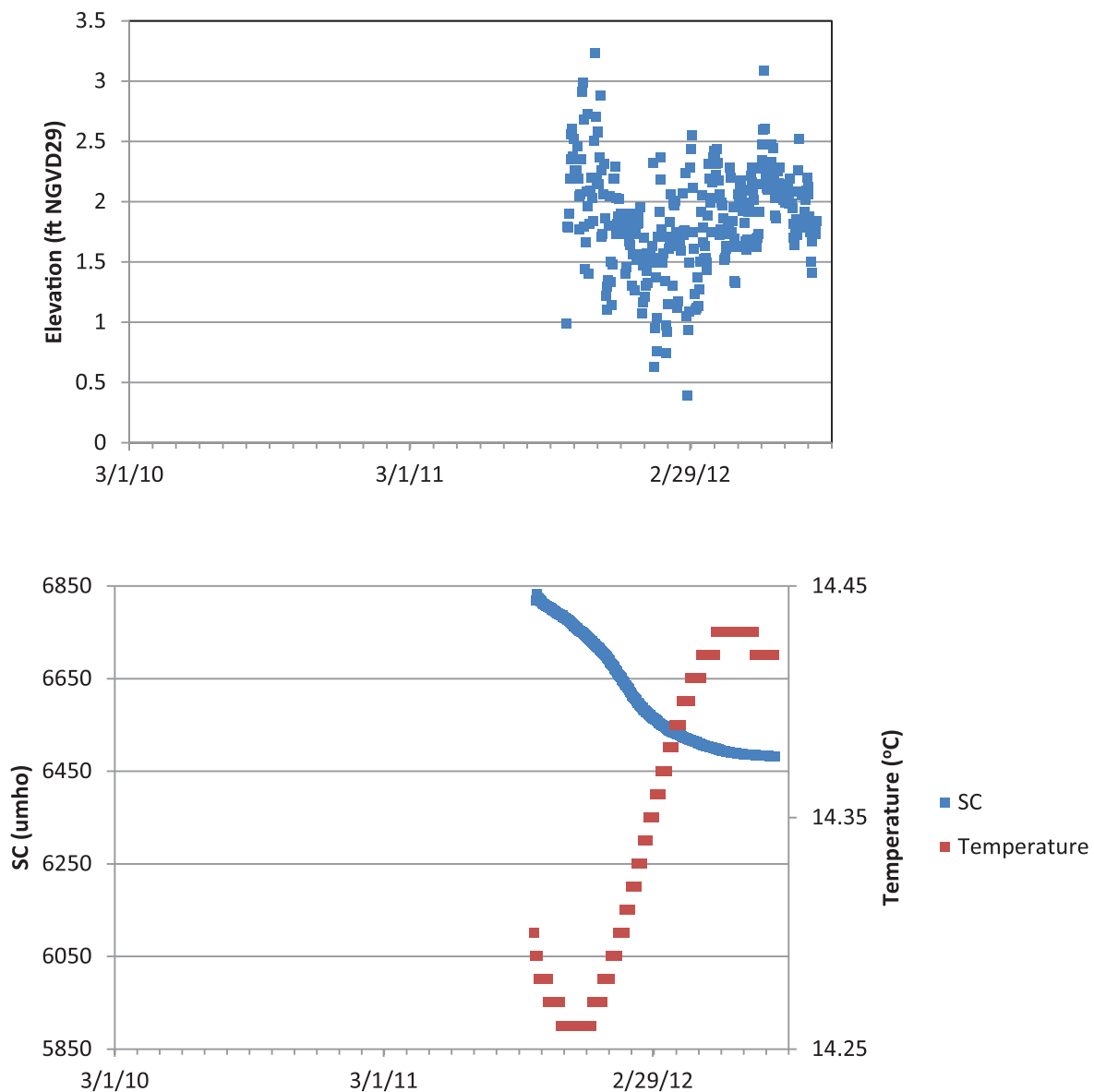


Figure B7. Hydrograph, thermograph, and specific conductivity graph for F2 (Pi53-11).
 NGVD29-National Geodetic Vertical Datum of 1929
 SC-specific conductivity
 umho-micromhos

APPENDIX B

HYDROGRAPHS, THERMOGRAPHS, AND SPECIFIC CONDUCTIVITY GRAPHS FOR SELECT WELLS

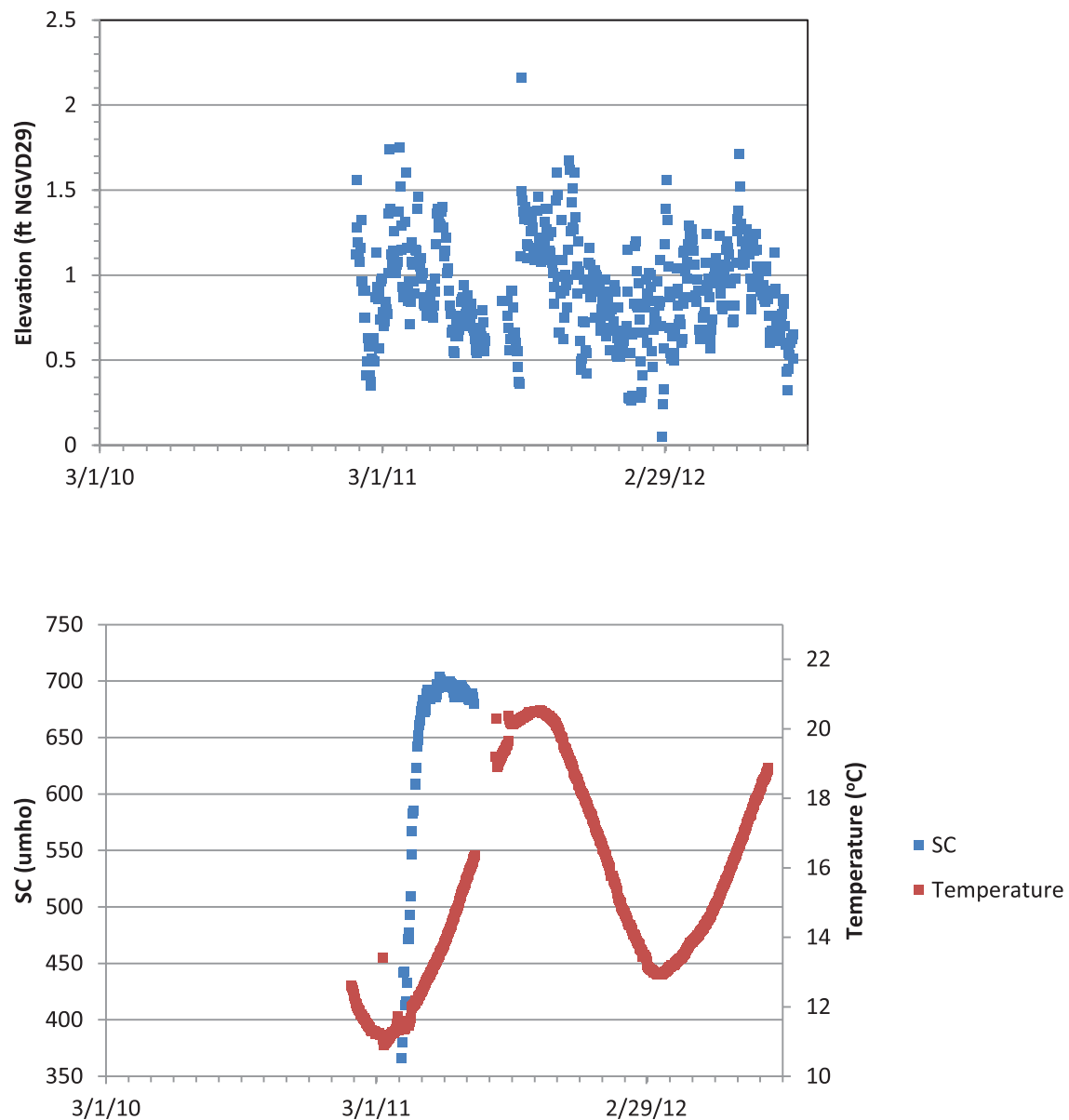


Figure B8. Hydrograph, thermograph, and specific conductivity graph for IN4 (Pi53-12).
NGVD 29-National Geodetic Vertical Datum of 1929
SC-specific conductivity
umho-micromhos

APPENDIX B **HYDROGRAPHS, THERMOGRAPHS, AND SPECIFIC CONDUCTIVITY GRAPHS FOR SELECT WELLS**

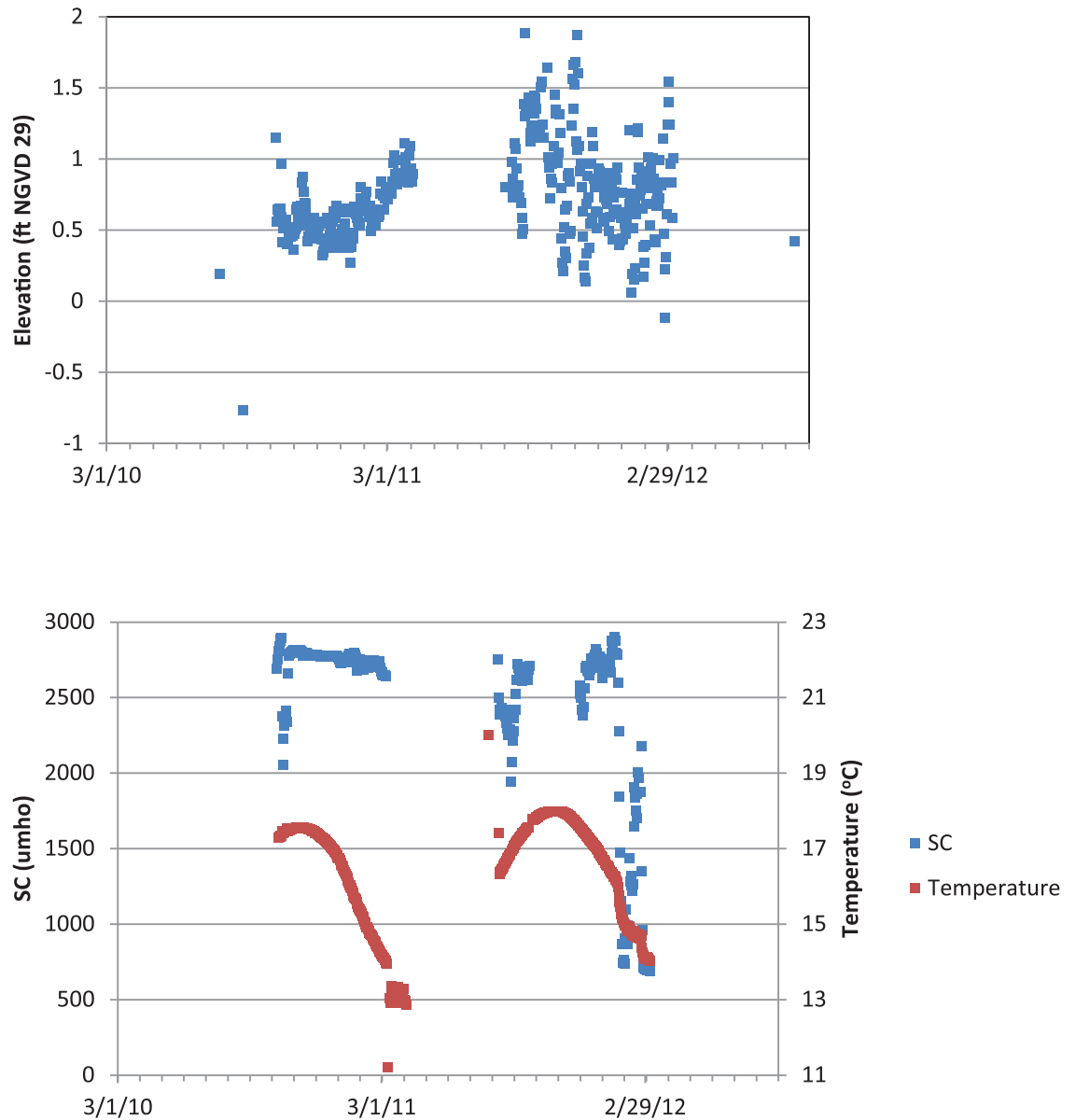


Figure B9. Hydrograph, thermograph, and specific conductivity graph for S9 (Pi53-13).
 NGVD29-National Geodetic Vertical Datum of 1929
 SC-specific conductivity
 umho-micromhos

APPENDIX B **HYDROGRAPHS, THERMOGRAPHS, AND SPECIFIC CONDUCTIVITY GRAPHS FOR SELECT WELLS**

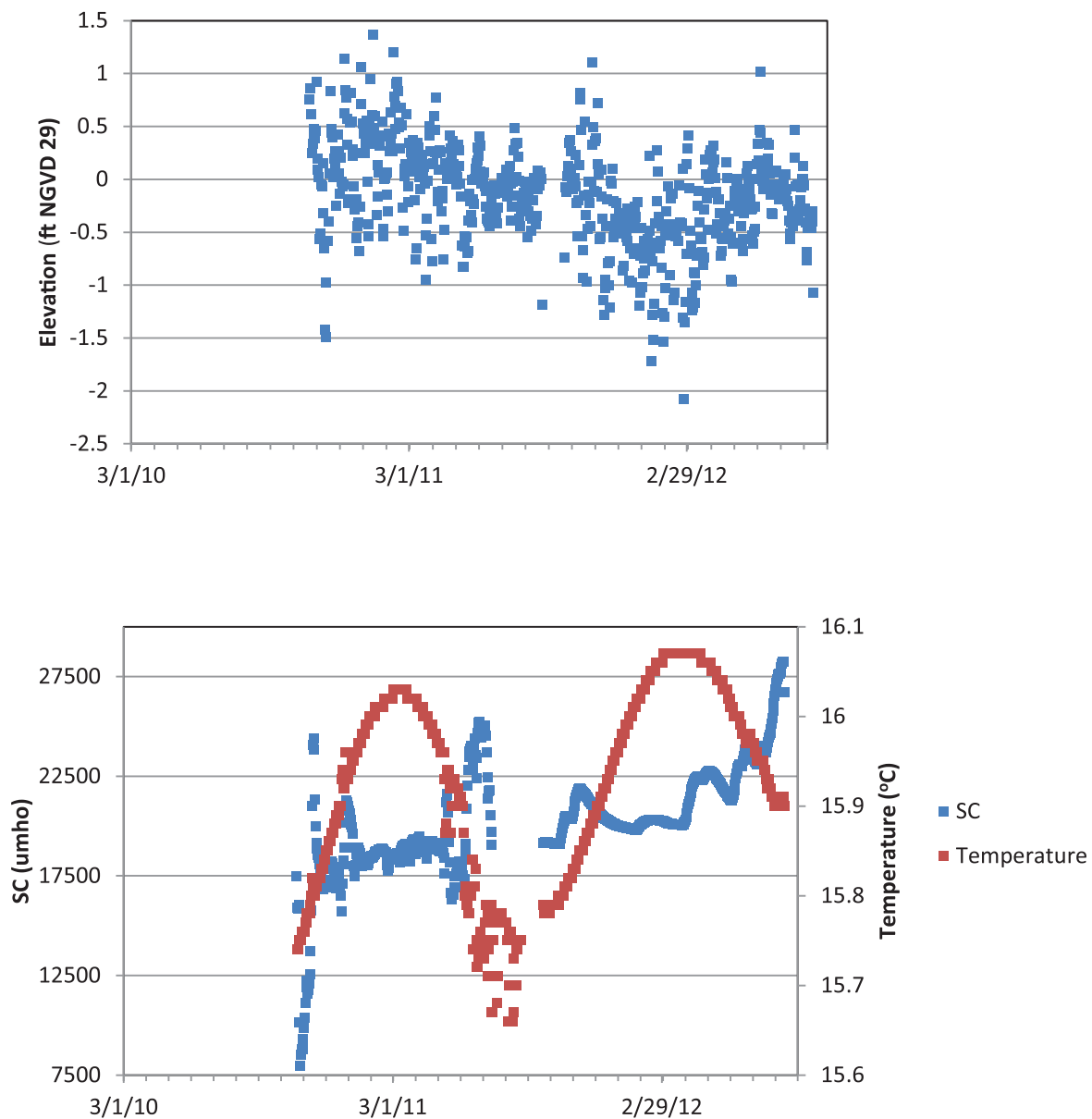


Figure B10. Hydrograph, thermograph, and specific conductivity graph for F3 (Pi53-14).
 NGVD29-National Geodetic Vertical Datum of 1929
 SC-specific conductivity
 umho-micromhos

APPENDIX B

HYDROGRAPHS, THERMOGRAPHS, AND SPECIFIC CONDUCTIVITY GRAPHS FOR SELECT WELLS

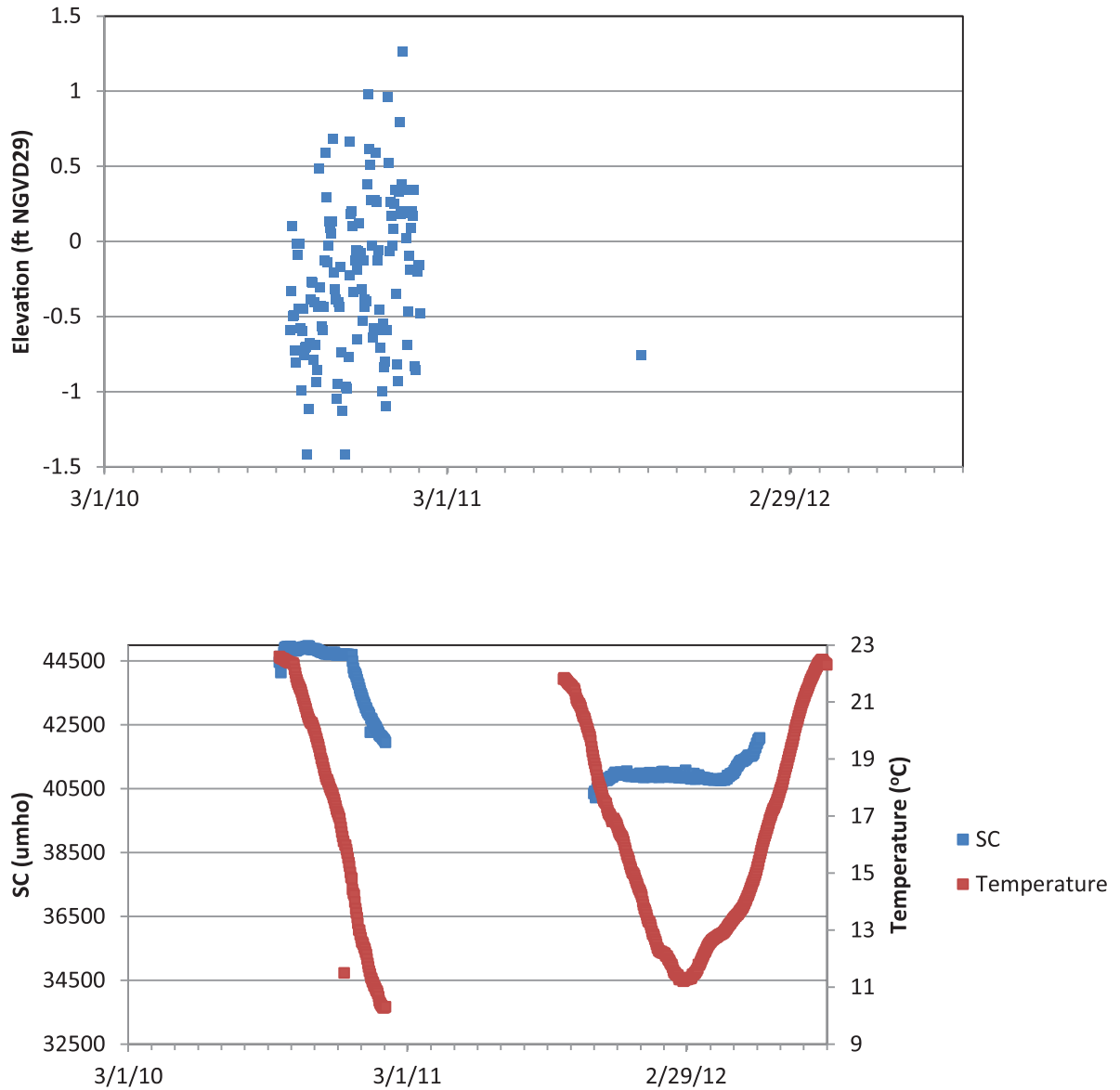


Figure B11. Hydrograph, thermograph, and specific conductivity graph for F4 (Pi53-15).
NGVD29-National Geodetic Vertical Datum of 1929
SC-specific conductivity
umho-micromhos

APPENDIX B

HYDROGRAPHS, THERMOGRAPHS, AND SPECIFIC CONDUCTIVITY GRAPHS FOR SELECT WELLS

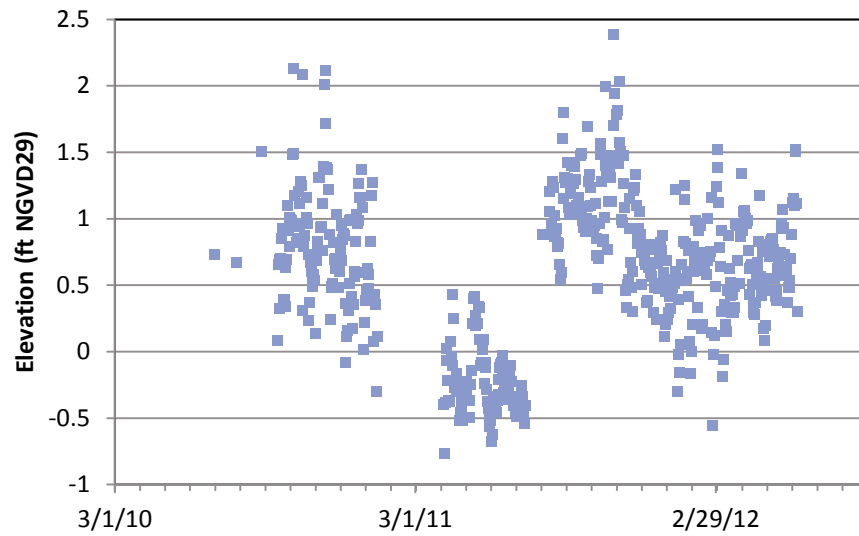


Figure B12. Hydrograph for S5 (Pi53-30).
NGVD29-National Geodetic Vertical Datum of 1929

APPENDIX B **HYDROGRAPHS, THERMOGRAPHS, AND SPECIFIC CONDUCTIVITY GRAPHS FOR SELECT WELLS**

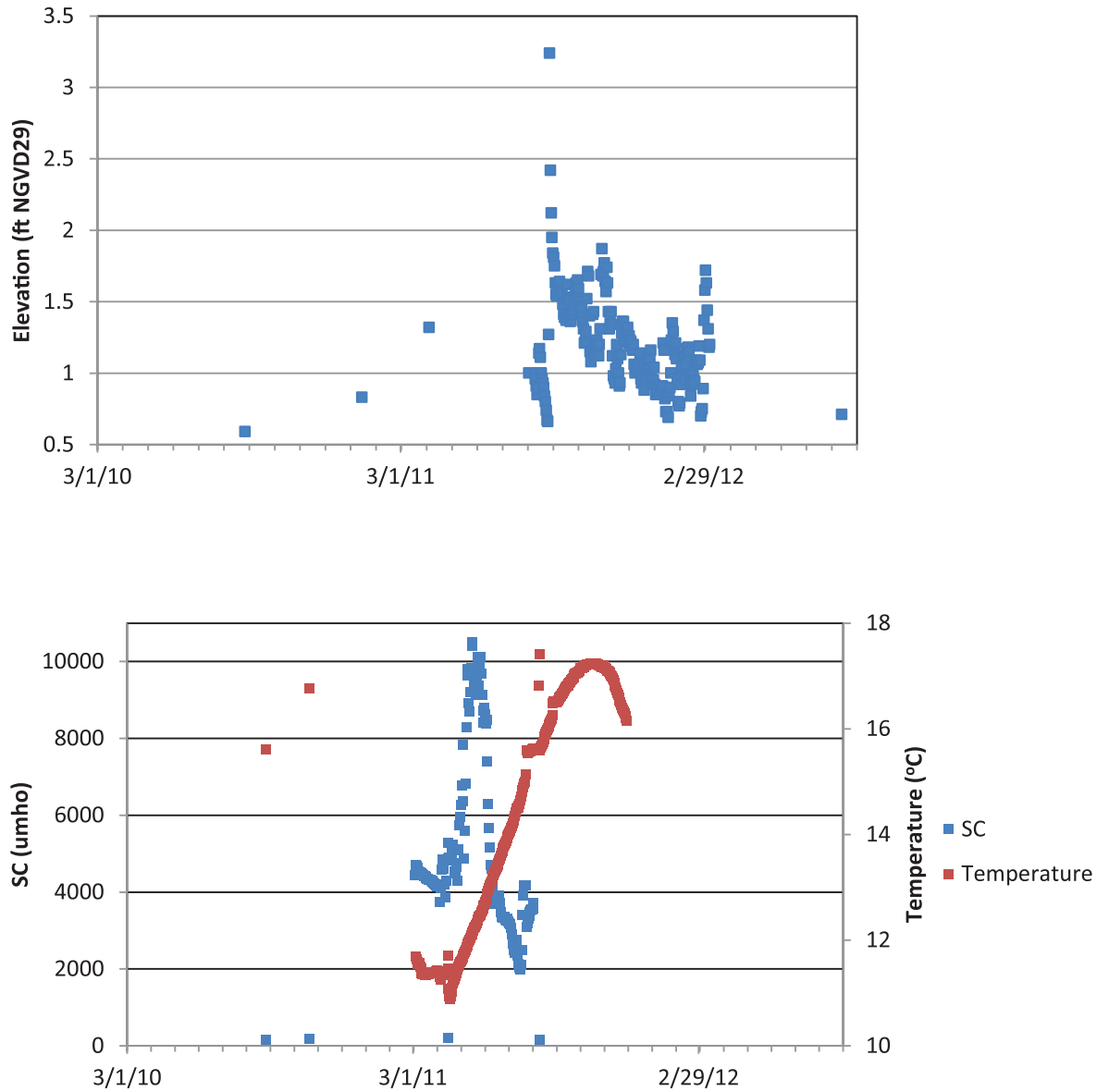


Figure B13. Hydrograph, thermograph, and specific conductivity graph for S7 (Pi53-51).
 NGVD29-National Geodetic Vertical Datum of 1929
 SC-specific conductivity
 umho-micromhos

APPENDIX B **HYDROGRAPHS, THERMOGRAPHS, AND SPECIFIC CONDUCTIVITY GRAPHS FOR SELECT WELLS**

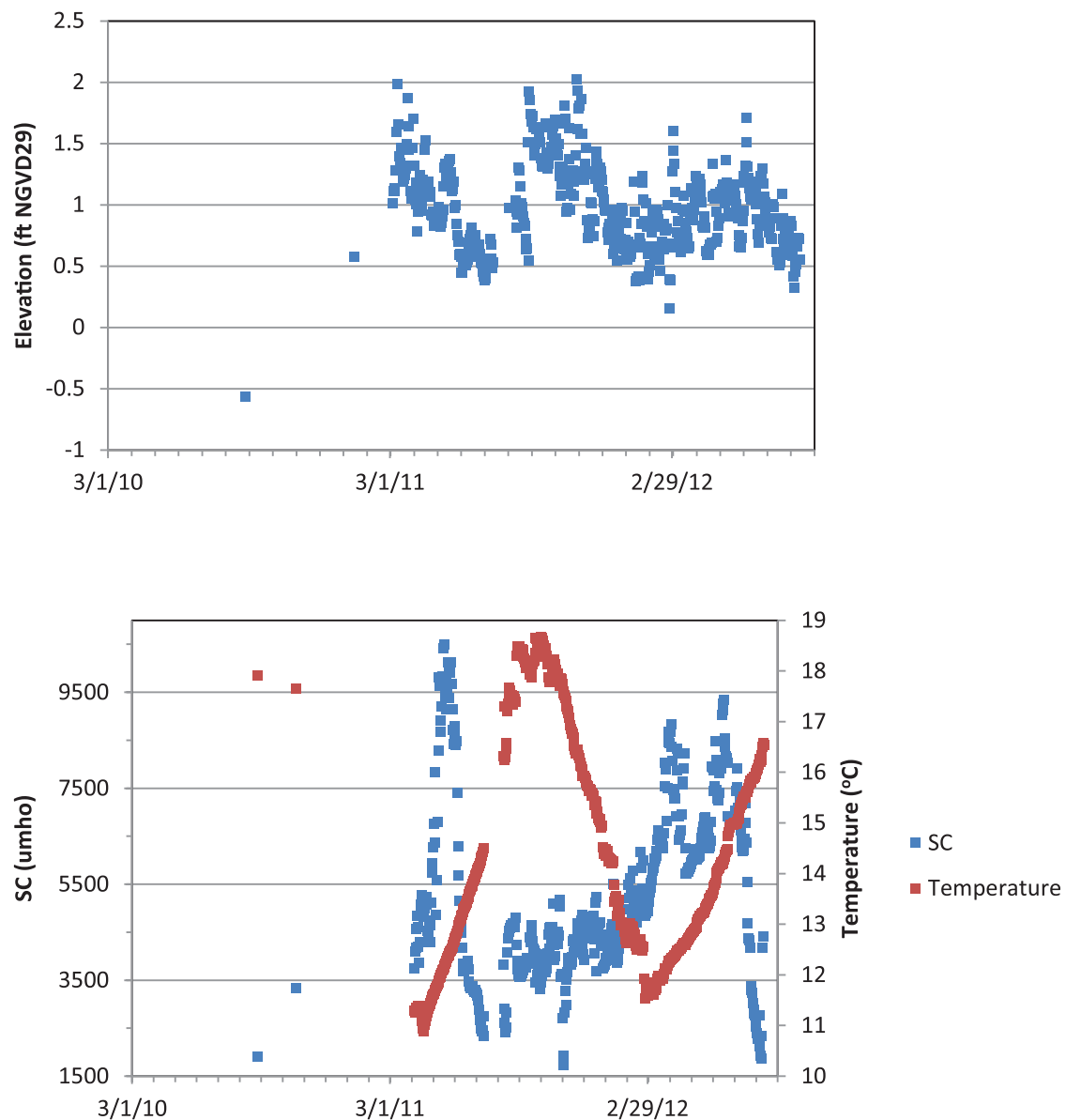


Figure B14. Hydrograph, thermograph, and specific conductivity graph for S8 (Pi53-52).
 NGVD29-National Geodetic Vertical Datum of 1929
 SC-specific conductivity
 umho-micromhos

APPENDIX B **HYDROGRAPHS, THERMOGRAPHS, AND SPECIFIC CONDUCTIVITY GRAPHS FOR SELECT WELLS**

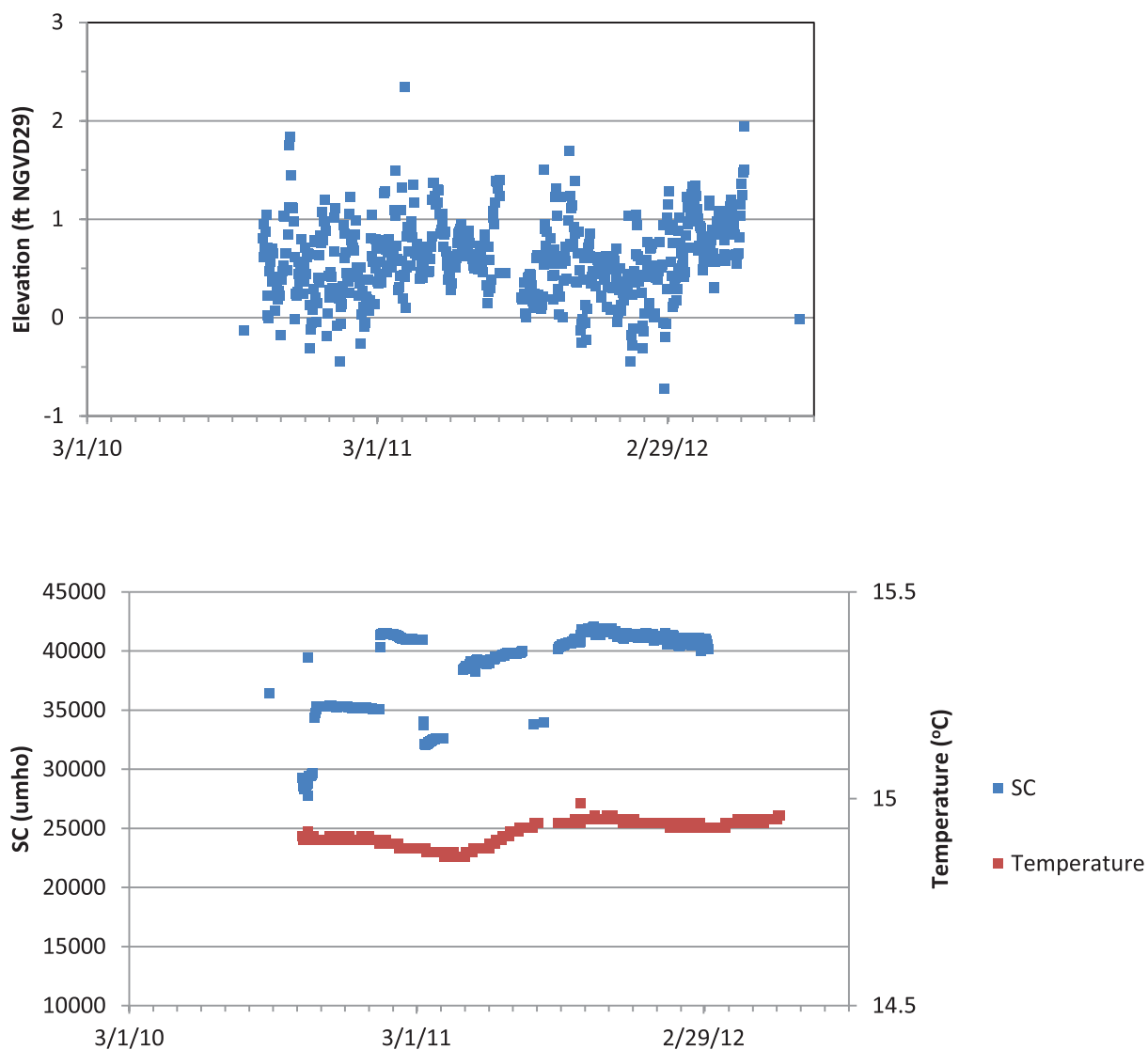


Figure B15. Hydrograph, thermograph, and specific conductivity graph for S6 (Pi53-53).
 NGVD29-National Geodetic Vertical Datum of 1929
 SC-specific conductivity
 umho-micromhos



Delaware Geological Survey
University of Delaware
Newark, Delaware 19716